Politecnico di Torino

Master's degree in Environmental and Land Engineering

Graduation session:

July 2025

Green synthesis of nanostructured catalysts for electrochemical reduction of CO_2 to valuable products

SUPERVISORS :

Prof. Zeng Juqin

Prof. Pirri Candido

Candidate :

Ali Shadervan

(ID : S315409)

Contents

Introduction

CO_2 gas, which is produced through natural and artificial processes, is considered a very important gas for the growth of plants as well as the activity of some industries. Ideally, the amount of production and consumption of this gas in nature should be in balance. But today, due to the increase in industrial activities, this balance has been disrupted, and we see a significant increase in the amount of this gas in nature. CO_2 is an inactive substance due to its harmony in its chemical structure, and it has more retention in nature than CO_2. Even in its high concentrations, the air composition constitutes only a small percentage of this substance. But even this small percentage has many environmental effects due to their function in absorbing and emitting infrared radiation in the atmosphere.[1]

The increasing levels of carbon dioxide (CO_2) in the atmosphere has an major environmental impact due to their contribution to global warming. The primary reasons of the increase in atmospheric CO_2 concentrations are the combustion of fossil fuels, deforestation, agricultural practices, or the production of cement, which play a main role in the increase of CO_2 concentration in the atmosphere.[2]

The greenhouse effect is one of the most destructive challenges facing humanity because it makes the gradual increase of the atmospheric temperature, known as global warming, and can lead to undesirable climate change and the extinction of species. [3]

CHAPTER 1

1. Carbon Dioxide Electroreduction: *an overview*

1.1 The Greenhouse Effect and CO_2 Mitigation Strategies

in today's world the overuse of fossil fuel is inevitable to support the progress and this leads to over CO_2 emission. Even with the rising climate change abating policies, total GHG emissions rose on average by 1.0 $GtCO_2$-eq (2.2%) annually, in 2000-2010, compared to 0.4 $GtCO_2$-eq (1.3%) annually, in 1970-2000 (Fig 1-1). [3, 4]

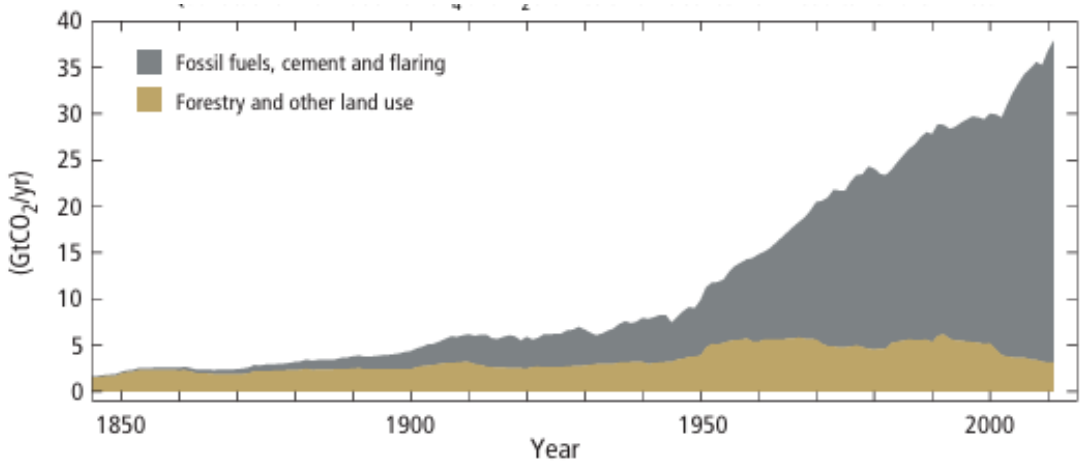

Figure 1-1 Annual global anthropogenic carbon dioxide (CO_2) emissions (gigatonne of CO_2-equivalent per year, $GtCO_2$ /yr) from fossil fuel combustion, cement production and flaring, and forestry and other land use , 1750–2011[3]

The Earth's atmosphere is crucial to maintaining Earth warm by trapping the Sun's heat. This natural phenomenon, also known as the greenhouse effect, is primarily attributed to gases such as carbon dioxide (CO_2), methane (CH_4), nitrous oxide (N_2O), ozone (O_3), and water vapor (H_2O). Even though vitally important to sustaining life, excessive emission of greenhouse gases (GHGs) has had severe environmental consequences such as global warming, sea-level rise, and extreme weather events.[5]

Among the strongest motivators for these shifts is anthropogenic CO_2 emissions, which are largely driven by fossil fuel combustion, industrial activity, and land use changes. Various ways have been proposed to mitigate CO_2 emissions, including carbon capture and storage (CCS), direct air capture

(DAC), and carbon utilization. These encompass CO_2 conversion and utilization into useful chemicals and fuels as particularly promising alternatives based on their potential for environmental sustainability and economic feasibility.[5, 6]

1.2 CO_2 molecule structure

CO_2 is odorless and colorless gas, and its density at standard pressure and zero degree centigrade is 1.9 kg/m3 that is close to 1.5 times the air density. CO_2 molecule consists of two double bonds with a linear shape. CO_2 is not electric dipoles and is completely oxidized and non-combustible. Solid CO_2 sublimates at 194.7 K and melts at a pressure of more than 5.2 bar. The triple point of this compound is at a pressure of 5.2 bar and at a temperature of 216.6 k. The critical point of CO_2 is 73.8 bar and 304.1 k. .[7]

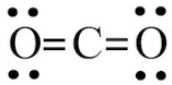

Figure 1-2-CO_2 structure[7]

Structurally, the gas is a linear molecule, and the C-O bond length is abot 116.3 pm consisting of sigma and pi bonds. The two pi bonds are perpendicular and polarized as any carbon-oxygen bond, with a positive partial charge on the carbon atom and negative partial charge on oxygen.[8] . CO_2 is the most oxidized carbon, thus the only way to reduce it chemically at normal energy levels; It is to reduce it. Through donation of an electron, the geometry of CO_2 becomes bent from linear and is irreversibly reduced.[9]

1.3 Methods for decreasing the amount of CO_2

One of the ways CO_2 can be reduced is through direct and indirect storage and absorption, an example of which occurs naturally as limestone, where calcium oxide absorbs CO_2 from the environment and transfers it into calcium carbonate, thereby producing billions of tons of stored CO_2 in natural minerals.[10, 11]

One of the right methods to mold a carbon-free world is to evolve a carbon cycle and use CO_2 as a raw material for the synthesis of consumer products which can be used effectively as a substitute for fossil resources. In the following figure, it is shown that for this purpose, an effort is made to employ renewable sources like the sun, wind energy and other natural components.[12]

Table 1-1- Treatment for CO_2 mitigation[9]

Treatment method	Characteristic	Drawback
Higher efficiency in electric energy production	• Use of innovative technologies usually • Efficiency improvements from 30% to 53% (IGCC)	High costs and long implementation times
Utilization of energy with better efficiency	• Requires a more conscientious attitude towards energy usage • Methods such as driving more fuel-efficient vehicles, using electrical appliances more efficiently	Difficult to plan and control in a unified manner
Fuel shift	From coal to gas Coal (950) > oil > gas (497)	Distribution of resources
Carbon capture and storage (CCS)	• Large potential in CO_2 storage Storage in natural fields • Not accepted by many countries	Security and economic (costly, uncertainty, intensive energy requirements)
CO_2 conversion and utilization	• Recycles carbon • Reduces the extraction of fossil-C • Avoids emission of CO_2	

1.4 Methods for conversion of CO_2

Different routes have been suggested for the transformation of CO_2 to valuable compounds, which fall into four broad chemical, photochemical, photochemical, and photoelectrochemical categories, and are given below.[13]

1.4.1 Chemical methods:

In chemical methods, there are two types of homogeneous and heterogeneous catalysts used. In chemical methods with a homogeneous catalyst, with the action of hydrogen gas and with proper experimental conditions, CO_2 is converted into different products such as methanol, methane and formic acid. methanol is the most important among these products. The key to converting CO_2 to the aforementioned products, is to employ an appropriate catalyst to form products at a high rate. While several homogeneous catalysts have been studied to convert CO_2 to methanol, examples of such catalysts are limited.[14]

1.4.2 Photochemical methods:

Photo chemical or photo catalytic reactions are generally utilized to downgrade stored CO_2 to methanol and other valuable products using solar energy. Photo catalytic conversion of CO_2 encompasses a combination of photo physical and photo chemical reactions. Owing to the fact that molecular catalysts are utilized, photo chemical reactions are relatively equivalent to electro catalytic reactions.[15]

Typically, sacrificial hybrid sources are applied as a determinant for CO_2 reduction based on photochemical means. Ascorbic acid amine and 1-benzyl-4 and 1-dichloronicotide amine are a few among the hybrid sources that have to be added in the solution to act as anodes in electrocatalytic means.[16]

1.4.3 Photo elechtrochemical methods:

Photo electrocatalytic or photo electrochemical CO_2 reduction is an integration of electrocatalytic and photocatalytic processes. Scientists are particularly interested in semiconductor compounds that are to be used as photo anodes in cells called PEC (photoelectrochemical cells) to decrease CO_2 to valuable compounds such as fuel with the help of solar radiation.[17]

The photoelectrochemical reaction thermodynamically requires approximately 1.5 eV of energy. Therefore, the PEC cell is utilized to counteract the energy of surface charge separation at the semiconductor surface, overvoltage, and resistance. It takes more energy. [18]

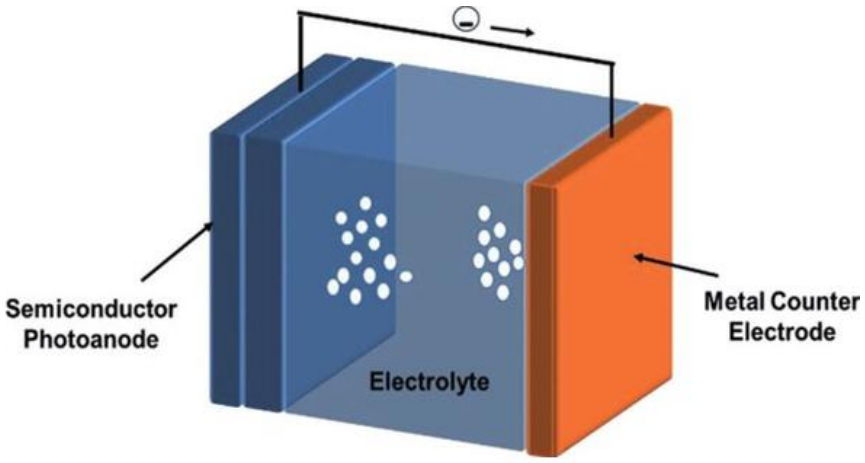

Figure 1-3- photoelectrochemical cell[19]

1.4.4 Electrochemical method:

Currently, the electrochemical synthesis process or electrosynthesis of valuable compounds from cheap materials is being widely used and utilized in many industries. Electrosynthesis is a method through which various chemical compounds are synthesized due to electron exchange between the solution/electrode. The best conditions for electrosynthesis are provided if a suitable and optimal mixture of solvent and electrolyte is used and electric resistance of the solution is minimized. Under the electrosynthesis process, useful chemicals are generally produced at room pressure and temperature without any modification of toxic test reagents. This process is carried out at low energy, from which the target molecules are synthesized easily with lower cost and cheap reagents. This process is generally utilized in the process of green chemistry, as from this process a large number of harmful and destructive molecules like CO_2 are transformed into non-destructive and

even useful and valuable products using very little energy. One of the major applications of the electrosynthesis process is the electrochemical reduction of CO_2 and its transformation into materials of the chemical as well as fuel industries.[20]

Electrochemical CO_2 Reduction (CO_2RR) and Its Importance:

Electrochemical reduction of CO_2 (CO_2RR) is a green technology that seeks to reduce CO_2 to valuable products like carbon monoxide (CO), formic acid (HCOOH), hydrocarbons, and alcohols from renewable electricity. CO_2 reduction not only solves the issue of CO_2 emissions but also allows for the generation of sustainable chemicals and fuels.[21]

The fundamental reaction of CO_2RR occurs at the cathode of an electrochemical cell, following the general reaction:

$$\boldsymbol{xCO_2 + nH^+ \longrightarrow products + yH_2O} \quad \text{Equation 1-1}$$

One of the greatest challenges with CO_2RR is overcoming the high energy barrier for the activation of CO_2, requiring an effective catalyst to drive the reaction without sacrificing high selectivity and efficiency. Another great challenge that comes with CO_2RR is competition with the hydrogen evolution reaction (HER), where HER often occurs at similar potentials, reducing the overall efficiency of CO_2RR.[22]

Several studies have been conducted on the employment of different electrocatalysts and the application of different experimental conditions, and it has been observed that the character of the catalyst and the reaction conditions play a significant role in deciding the level of applied potential employed during the synthesis of a specific product.

But HER hydrogen release reaction requires equal potential and energy as CO_2 reduction. For this, an effort is made to employ electrodes with high potential compared to HER.[23]

In the electrochemical process, three-electrode cell electrolysis is widely followed. CO_2 electro-chemical reduction (ECR) is an electrochemical process in which multiple-step reaction follows

where generally in the reduction step; Two, four, six or eight electrons or more are exchanged. This takes place between the CO_2 saturated electrode/electrolyte. In general, this catalytic process is explained in three main steps:

1. Chemical adsorption of CO_2 over the electrocatalyst surface

2. Proton transfer or electron migration to break the C-O bond or form C-H

3. Rebuilding of the product structure and their desorption from the electrode to the electrolyte

Outer structure of CO_2 electrolysis cell is much similar to the cells for water electrolysis using proton exchange membrane PEM, which is used to purify hydrogen gas. The desired membrane is usually composed of neutral materials that allow passage of only the electrolyte and not gaseous product transportation. In PEM electrolysis cells, the membrane acts as the proton conductor in such a manner that the hydrogen ions produced at the anode diffuse through the membrane, Aside from performing a role in CO_2 recovery, they react in the cathode and produce hydrogen gas. For CO_2 regeneration, electrode and electrolyte design in the anodic side is the same as water electrolysis system but for the cathodic side; Electrode formulation and electrolyte formulation change depending on product type to be generated.[24]

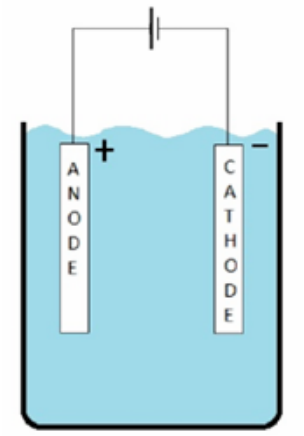

Figure 1-4- electrochemical cell[24]

Theoretical and thermodynamic study of CO_2 electrochemical reduction reaction:

There are several kinematic and thermodynamic barriers to effectively transform CO_2 into valuable products. CO_2 is highly stable molecule in the thermodynamic point of view and has a heat of formation of precisely -394.39 $kjmol^{-1}$. Therefore, activation of this material and its participation in chemical reactions is a very difficult task from the thermodynamic point of view.[25]

Therefore, stimulating this substance and its participation in chemical reactions is a very difficult task in terms of thermodynamics. From a theoretical and thermodynamic point of view, the conversion of CO_2 is possible, and according to the data in the table, for example, CO_2 is converted to methane by receiving 8 electrons and protons at a -0.24 vs. RHE. But from a practical and kinematic point of view, due to the formation of energetic intermediates with high kinetic barriers, it is difficult to perform this process.[13]

Eo is the normal potential relative to the standard hydrogen electrode at standard conditions in a solution with a pH equal to seven at 25 C and pressure of 1 atmosphere[13]. As one-electron reduction of CO_2 to $CO_2^{-\cdot}$ radical would require a structural reconstruction from linear to bent, therefore 2ev of free energy or a corresponding potential to -1.9v relative to RHE is needed. On the other hand, the equivalent reduction of a specific carbon dioxide change can be attained through hydrogen addition (donor) or electron transfer to reduce the thermodynamic energy barrier.[25]

Therefore, a suitable and efficient electrocatalyst needs to be employed to execute the electrochemical reduction process of CO_2 and convert it into useful products. A perfect electrocatalyst not only supports electron transfer but also maximizes the rate of the chemical reaction. In addition, a perfect electrocatalyst supports an ideal thermodynamic match between the electron transfer standard reduction potential and the chemical reaction of the catalyst.[26]. The Electro-chemical reduction(ECR) possesses different multi-proton and multi-electron transportation processes with 2, 4, 6, 8 and 12 electron paths [26]. Thus, a list of useful chemicals (e.g., CO, CH_3OH, CH_4, HCOOH, C_2H_4, and HCHO) will result from varying reaction routes being employed [9]. We present a list of half reactions and their electrode potentials that occur in electro-chemica reduction in Figure (1-5).

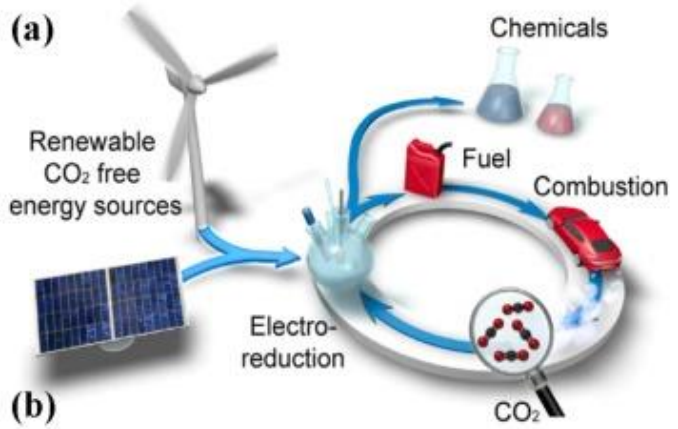

(b)

CO_2 Reduction Half Reactions			[V] vs RHE
$CO_2 + H_2O + 2e^-$	→	$CO + 2OH^-$	-0.10
$CO_2 + H_2O + 2e^-$	→	$HCOO^- + OH^-$	-0.03
$CO_2 + 5H_2O + 6e^-$	→	$CH_3OH + 6OH^-$	0.03
$CO_2 + 6H_2O + 8e^-$	→	$CH_4 + 8OH^-$	0.17
$2CO_2 + 8H_2O + 12e^-$	→	$C_2H_4 + 12OH^-$	0.08
H_2O Reduction Half Reaction			
$2H_2O + 2e^-$	→	$2H_2 + 2OH^-$	0.0

Figure 1-5 (a) Illustration of an artificial way of carbon recycling powered by renewable electricity sources such as wind and solar. (b) Several representative half reactions and reduction potentials of CO_2 reduction reactions, along with that of the HER.[27]

When the process of CO_2 recovery is varied in the environmental conditions, one can vary the faradaic efficiency and the type of product. Faraday efficiency is a measure of how well the charge used in the electrochemical process is converted into useful products. To determine Faradaic efficiency FE, initially the number of electrons passed through the solution (considering the base line) is determined from the area below the peak of the voltammetric curve. Next, the amount of the product is determined. By multiplying the quantitative value of the product with the quantity of electrons that produce it, the yield value is obtained.[28]

The calculations needed are done via the following relationships, where I is the flow intensity; t is the time to perform the process of ECR; Q_{theo} quantity of passed charge in the electrolysis process; Q_{exp} quantity of charge expended to produce the desired product; n is the number of moles of electrons to produce the desired product; F is the Faraday constant and p is the product.[27]

$Q_{\text{theo}} = I.\text{t}$ Equation 1-2

$\boldsymbol{Q_{exp} = \pi.\text{F}.mol_p}$ Equation 1-3

$FE(\%) = (\frac{Q_{exp}}{Q_{th}}) \times 10$ Equation 1-4

Theoretically, several factors are effective on the reaction of CO_2 regeneration and the type of product, which are closely related and are mentioned below.

ElectroCatalyst Design and Materials for CO_2RR

Design of the catalyst is the most significant factor in governing the efficiency, selectivity, and stability of CO_2RR from CO. Gold (Au) and silver (Ag) metals have a tendency to produce preferentially CO, but formate production is a preference for tin (Sn), lead (Pb), and bismuth (Bi). Copper (Cu) stands out in that it catalyzes multi-carbon (C_2^+) product formation such as ethylene (C_2H_4) and ethanol (C_2H_5OH) and therefore is a focus of interest for CO_2RR research.

Several factors influence the activity of the catalyst, including [29]:

- Nanostructuring and morphology: The shape and size of nanoparticles affect activity as well as selectivity.
- Bimetallic and alloy catalysts: Synergistic effects can be attained by alloying Cu with metals like Ag, Zn, or Bi for better CO_2RR performance.
- Surface modification: The catalytic performance may be significantly altered due to doping, defect engineering, and control of oxidation states. Cu-Ag type bimetallic Cu-based catalysts have been explored in recent studies to promote CO adsorption and facilitate C-C coupling for C_2 product formation. These materials utilize the "tandem effect" in which Ag first reduces CO_2 to CO, followed by Cu further reducing CO to C_2^+ products[30].

Advantages of nanostructured catalysts

Nanoparticles introduce unique advantages in carbon dioxide (CO_2RR) electrochemical reduction due to their high surface area-to-volume ratio, readily tunable electronic characteristics, and high density of active catalytic sites. These properties enhance catalyst-reactant molecule interactions and hence improve catalytic activity and selectivity [31]. For example, copper and bismuth nanoparticles, especially sulfur- or tin-doped counterparts, have shown better performance in lowering CO_2 to useful products such as formate and carbon monoxide. Sulfur doping specifically improves undercoordinated active sites, and intermediate binding is tuned to be optimal, thus enhancing formate formation and suppressing side reactions such as hydrogen evolution.[32]

Furthermore, electrocatalysts with nanostructures like Cu–Sn foams and Sb–Cu_2O materials possess hierarchical porosity to facilitate mass transport and electron transfer, leading to increased reaction rates and faradaic efficiency.[33]

These aspects emphasize the promise associated with engineered nanoparticles as the crux in the development of next-generation electrocatalysts for efficient CO_2 exploitation.

Electrolyzer Configurations and Their Efficiency

The efficiency of CO_2RR is also heavily determined by electrochemical cell design. Standard arrangements of electrolyzers are:

- H-Type Cells: These are simple-to-handle batch reactors with mass transport limitations and low current densities (<100 mA cm^{-2}). They are routinely used in school-level research work.
- Flow Cells: They use gas diffusion electrodes (GDEs) to enhance mass transport and achieve higher current densities (>1000 mA cm^{-2}), making them suitable for large-scale industrial applications.
- Membrane Electrode Assemblies (MEA): These advanced designs optimize ion transport effectiveness and minimize crossover effects, enhancing overall CO_2RR performance.

- Solid Oxide Electrolysis Cells (SOECs): High-temperature operating cells offer higher kinetics and energy efficiency in CO_2 conversion to syngas (CO +H_2).[3, 34]

State-of-the-Art Advancements in CO_2 Electroreduction

Recent advances in CO_2RR have focused on catalyst stabilization, selectivity, and energy optimization. Some of the notable advances are:

- Nanostructured Cu catalysts: These materials optimize CO_2RR pathways by stabilizing crucial intermediates.[29]
- Bimetallic electrocatalysts (e.g., Cu-Ag, Cu-Zn, Bi-Sn): These systems utilize electronic as well as geometric effects to optimize formate and hydrocarbon selectivity..
- Electrolyte engineering: pH, ion composition, and buffer capacity modulations have been shown to affect reaction kinetics and product selectivity.
- Characterization methods at operating conditions: Some methods that have provided greater insight into catalyst surface modifications during CO_2RR include in situ Raman spectroscopy and X-ray photoelectron spectroscopy (XPS).

Bi-Cu bimetalic Catalysts for CO_2 Electroreduction

The need to combat rising atmospheric CO_2 levels led to the research for CO_2 conversion technologies, and one that has been found to be a sustainable and scalable choice is electrochemical CO_2 reduction (CO_2RR).

copper-based (Cu-based) catalysts have been found to be an exceptionally adaptable and interesting class of materials. Copper is the only transition metal that can reduce CO_2 into a broad diversity of products, ranging from short molecules like CO and formic acid to multi-carbon (C_2^+) products like ethylene, ethanol, and propanol. Although noble metals like gold and silver are selective towards CO formation, copper is the only one that allows for more extensive reduction with greater molecular complexity. Additionally Cu catalysts are Highly Tunable Nanostructure that can be structured into a wide variety of structures, dendrites, foams, and nanocrystals, to

optimize surface area, charge transfer, and stabilization of intermediates. For example, Cu–Sn foam catalysts have achieved as high as 94% Faradaic efficiencies for CO formation.[33] [35]

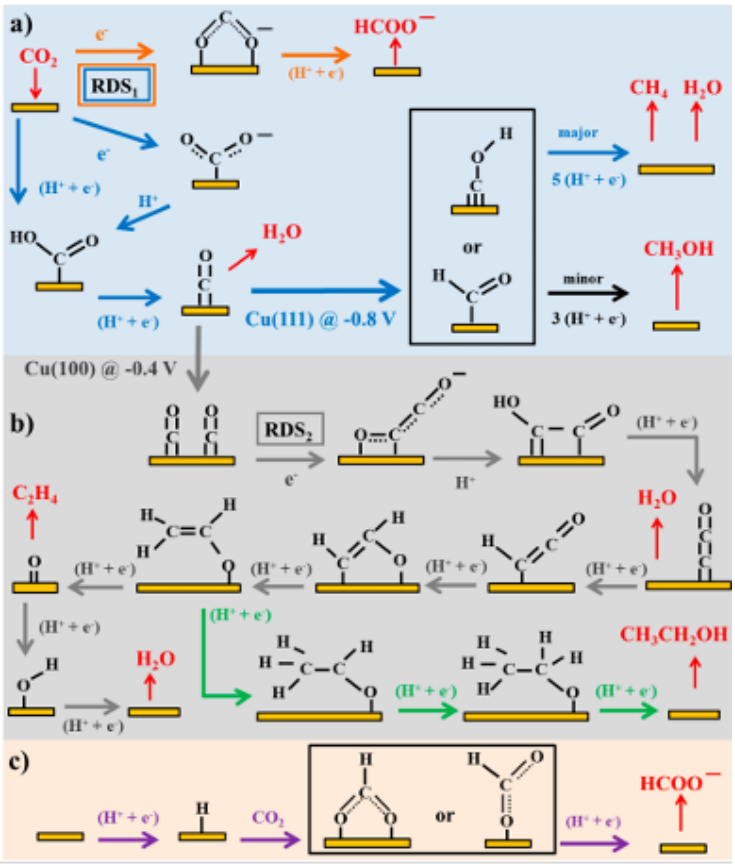

Figure 1-6- Reaction pathways on copper to (a) CO, CH_4, CH_3OH; (b) ethylene and ethanol; (c) formate [36].

Also Bismuth(Bi)-derived catalysts have proven efficiency and high selectivity in reducing CO_2 to formate/formic Acid owing to their good inherent catalytic activity and weak hydrogen bonding capability.[37] [38] [39]

1.5 Aim Of The Project

The goal of this project is to study the electrocatalytic activity of bismuth-modified copper-based catalysts for the reduction of carbon dioxide (CO_2) in an alkaline flow-cell system.

Bismuth was introduced to copper catalysts in varying concentrations to form a bimetallic system. The total catalyst loading remained constant at 1.67 mg/cm². Under varying conditions, electrochemical activity was examined using three various applied current densities: 100 and 200 mA/cm^2.

CHAPTER 2

2.Materials and Methods

2.1. Materials

Bismuth(III) nitrate pentahydrate ($Bi(NO_3)_3.5H_2O$, ≥98%), bismuth(III) chloride ($BiCl_3$, ≥98%), copper(II) chloride ($CuCl_2$, ≥99%), ethylene glycol (EG, 99.8%), and acetic acid (CH_3COOH, 99.8%, anhydrous) were purchased from Sigma-Aldrich. Nafion® 117 solution (5 wt.%) and isopropanol (≥99.5%) were supplied by Alfa Aesar. Potassium hydroxide (KOH, >85 wt.%) and sulfuric acid (H_2SO_4, 98 wt.%) were supplied by Merck. All chemicals were used without purification.

2.2. Catalyst synthesis

In a typical synthesis, 1 mmol of precursors were dissolved in 40 mL of EG, The precursor solution was then loaded into a Teflon vessel (volume 100 mL) that was placed in a microwave oven and connected to pressure and temperature probes (Milestone STARTSynth, Milestone Inc., Shelton, Connecticut) (Fig(2-1)). The Teflon vessel was then irradiated at 2, 5 or 10 min with controlled conditions (maximum temperature 180 °C and maximum power 900 W). The precipitate was cooled to RT, centrifuge-dreamed, washed twice with water and with ethanol once. The powder sample was finally gained by vacuum dry at 60 °C overnight.

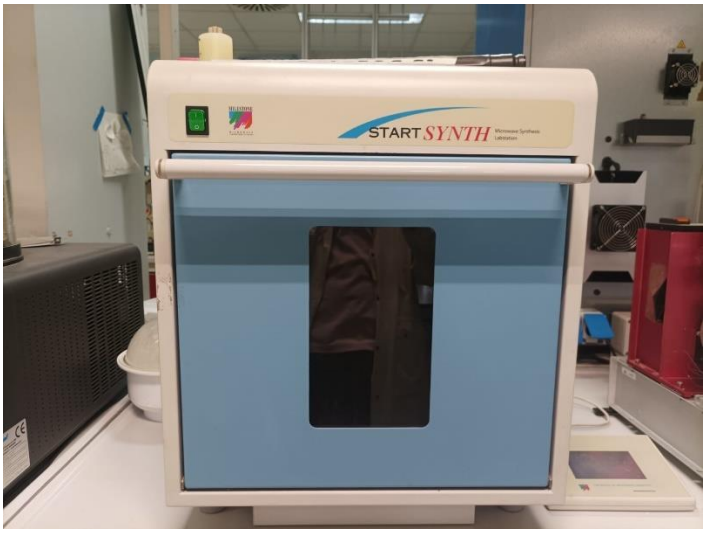

Figure 2-1- Microwave oven

2.3. Materials characterization:

In order to get a better insight into the catalyst's behavior in the electrochemical CO_2 reduction reaction (CO_2RR) and to elucidate the relationship between electrochemical activity and the material's physicochemical properties, it is crucial to perform detailed morphological, compositional, and structural analyses.

The following analytical techniques were employed in this study: Field Emission Scanning Electron Microscopy (FESEM; Supra 40, Zeiss, Oberkochen, Germany), Energy Dispersive X-ray Spectroscopy (EDS; Oxford Instruments, equipped with a liquid nitrogen-cooled Si(Li) detector), and X-ray Diffraction (XRD; PANalytical X'Pert Pro diffractometer with Cu-Kα radiation of 40 kV and 40 mA, equipped with an X'Celerator detector).

A brief overview of the equipment and underlying principles of each of the methods appears in the following sections.

2.3.1. Field Emission Scanning Electron Microscopy:

Field Emission Scanning Electron Microscopy (FESEM) is highly effective material analysis method since it possesses improved resolution (approximately 0.7-0.8 nm), large range of

magnification (20x to 10^6x), and greater depth of field compared to conventional optical microscopy. This is due to the fact that it uses a high-energy electron beam as the imaging source. From the De Broglie equation (equation (2-1)), their wavelength can be calculated from their kinetic energy (e.g., at 20 kV, the wavelength of an electron is around 0.027 nm). This very short wavelength allows for the nanoscale high-resolution imaging of material surfaces.

$$\boldsymbol{\lambda_{De\ Broglie}} = \frac{\boldsymbol{h}}{\boldsymbol{p}} \xrightarrow{\boldsymbol{E}=\frac{\boldsymbol{p^2}}{\boldsymbol{2m_c}}} \frac{\boldsymbol{h}}{\sqrt{\boldsymbol{2m_eE}}} \quad \text{Eq 2-1}$$

where:

h is the Planck's constant, $6.626 \cdot 10^{-34}$ J·s,

p is the electron momentum [kg· m/s],

m_e is the mass of one electron, $0.911 \cdot 10^{-30}$ kg.

In Field Emission Scanning Electron Microscopy (FESEM), the electron beam is produced at the upper part of the microscope column by an electron gun, which is powered based on the field emission principle. The mechanism relies on a very sharp tungsten (W) tip of single crystal. When a high voltage is applied between the cathode (the tungsten tip) and the anode, a very high electrostatic field is established. The electrons are expelled from the tip as a result of quantum tunneling. These electrons are much brighter than electrons emitted by thermionic emission, and FESEM is able to achieve much greater resolution.

The electron beam is focused and converged by two magnetic lens systems, namely the condenser lens and the objective lens. The beam is converged to a thin column by the condenser lens and then sharply focused onto the sample surface by the objective lens. Focal length is controlled by varying the magnetic field, which is achieved by varying the current in the lens.

To scan the sample surface, two sets of scanning coils deflect the beam in a raster scan. When the high-energy primary electrons from the beam impinge on the sample, they interact with the material and produce various signals e.g., secondary electrons (SE), backscattered electrons (BSE), Auger electrons, and X-rays. By detecting these signals, scientists can acquire extensive information on the surface morphology and chemical composition of the sample.

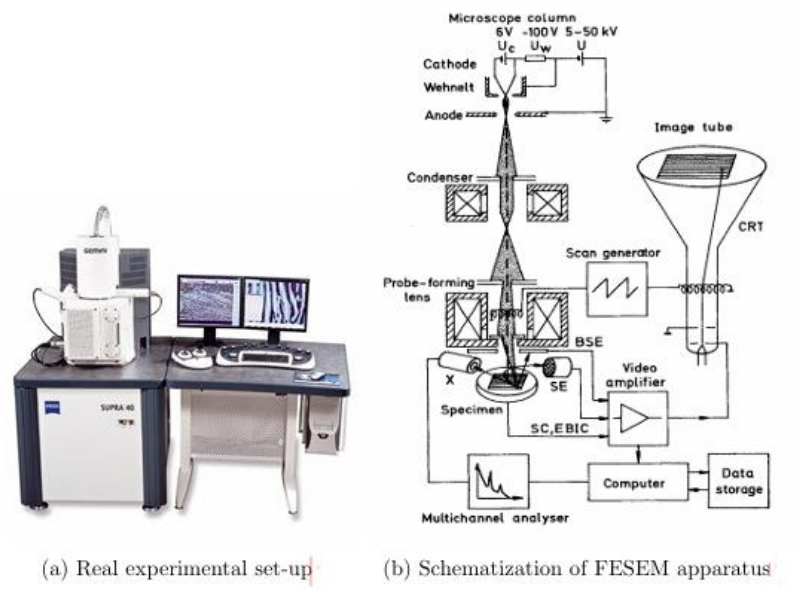

Figure 2-2 Real (a) and corresponding schematic (b) illustration of FESEM device.

Different detectors are normally included in a Field Emission Scanning Electron Microscope (FESEM) setup, each being specialized to collect particular types of signals. The Everhart-Thornley (E-T) detector, the solid-state detectors, and the In-lens detectors are most commonly used detectors. They are generally sensitive to backscattered electrons (BSE) and secondary electrons (SE).

The E-T detector is versatile and can be readjusted to sense SE by applying a positive voltage bias, or, though less commonly, BSE by applying a negative bias. BSE detectors are precisely calibrated for sensing BSE. In contrast to this, the In-lens detector is designed particularly for sensing SE alone.

The E-T detector employs a scintillator material (typically europium-doped CaF_2) that converts incident electrons to photons. The photons are passed into a photomultiplier tube (PMT), where they are reconverted to electrons. The resulting electron cascade is amplified and ultimately collimated at the anode, producing an electrical signal.

Whereas the E-T detector is positioned close to the sample at an angle to boost low-energy SE collection and preserve image depth, the In-lens detector is positioned within the objective lens

system. This position enables it to catch accelerated SEs, producing higher spatial resolution images, but with reduced three-dimensional information as a consequence of the lack of angular collection.

Four quadrants in solid-state detectors allow compositional as well as topographical analysis. Compositional data are obtained by combining signals from the four quadrants, and by comparing the differences (i.e., subtracting signals), surface topography can be reconstructed.

Morphological imaging was carried out in this work using the In-lens detector, chosen because of its increased spatial resolution.

2.3.2. Energy Dispersive Spectroscopy

Energy Dispersive X-ray Spectroscopy (EDS or EDX) is a widely used technique for determining the qualitative and quantitative chemical constitution of a material. It is based on measurement of X-ray photons produced by a sample following excitation by a high-energy beam of electrons. By incorporating an appropriate X-ray detector into the FESEM equipment, EDS analysis can be directly carried out as part of the electron microscopy technique.

When it collides with the atoms in a sample, it possesses sufficient energy to eject inner-shell electrons and leave vacancies in the core energy states of an atom. One of the electrons moves to replace the vacancy to achieve stability and emits an X-ray photon of energy corresponding to the two energy states involved. These photons are so called because their energies are fixed for an element and are effectively an individual fingerprint which can be used to identify an element. They appear as sharp peaks in an EDS spectrum.

In addition to characteristic radiation, continuum or so-called Bremsstrahlung radiation (Figure (2-3)) is also produced by the collision, which is responsible for the background of the spectrum. This is because the original electrons slow down when approaching atomic nuclei and produce a broad spectrum of lower-energy X-ray emissions.

In this application, the EDS detection uses a p-i-n semiconductor detector, normally cooled to cryogenic temperatures to reduce noise. X-ray photons striking on the detection surface produce

electron-hole pairs and produce an electrical signal of amplitude linearly related to photon energy. Since such a signal's amplitude is measured as a function of photon energy, a spectrum is obtained.

Position of peaks on the x-axis of the spectrum identifies which elements are present (qualitative analysis), and peak heights provide an approximate quantity of elements present (quantitative analysis), with a detection limit of around 1 atomic percent.

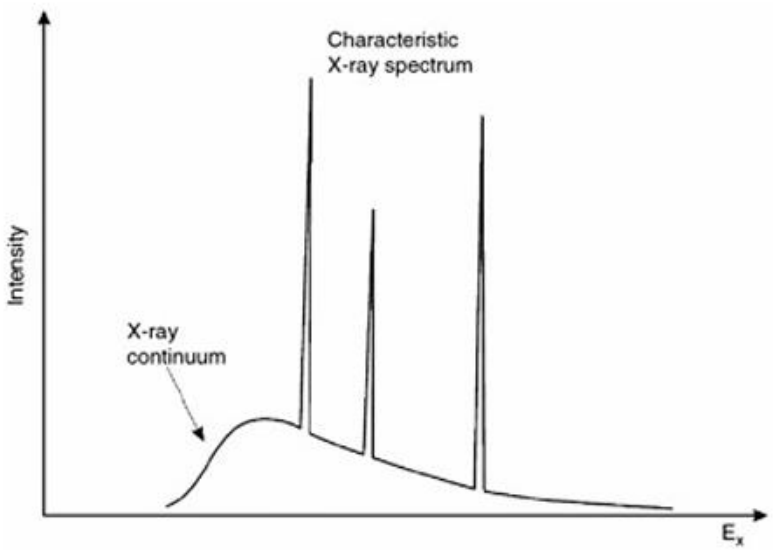

Figure 2-3 Typical EDX spectrum (Intensity of signal-Energy of X-ray photons)

2.3.3. X-Ray diffraction analysis:

X-Ray diffraction analysis is based on the Bragg's law:

$$n\lambda = 2dsin\theta \quad \text{Eq 2-2}$$

Where:

n is the order of diffraction, integer number (typically 1 or 2),

λ is the incident X-ray wavelength [nm],

d represents the interplanar distance [nm],

θ is the diffraction angle [degrees, °].

When the condition specified by Equation 2-2 is satisfied, a specific crystal plane with Miller indices (hkl) produces a diffraction pattern. That is, constructive interference arises, as the X-ray wavelength is equal to the optical path difference of the waves—written as 2dsinθ. This is illustrated in Figure 2-4.

In order to observe this diffraction, we require an X-ray diffractometer (Figure 2-5). As we previously discussed, X-rays are generated when a beam of electrons of great energy collides with a metal target (most often copper) within an XRD machine. This causes the metal to emit characteristic X-rays, known as Kα and Kβ radiation, which strike the sample.

If these conditions are satisfied according to Bragg's law, the resulting XRD pattern will be a plot of intensity versus 2θ with discrete peaks. Each peak is a consequence of diffraction by some set of crystal planes within the material and allows for determination of crystal structure.

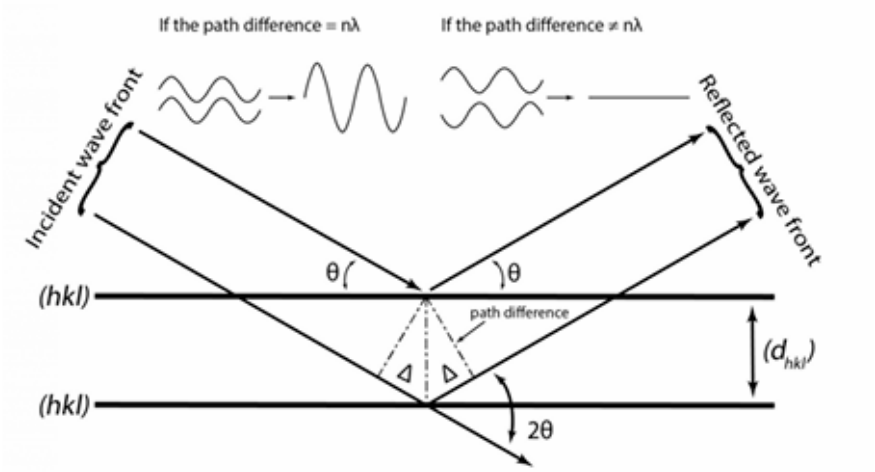

Figure 2-4 Schematic representation of X-ray diffraction

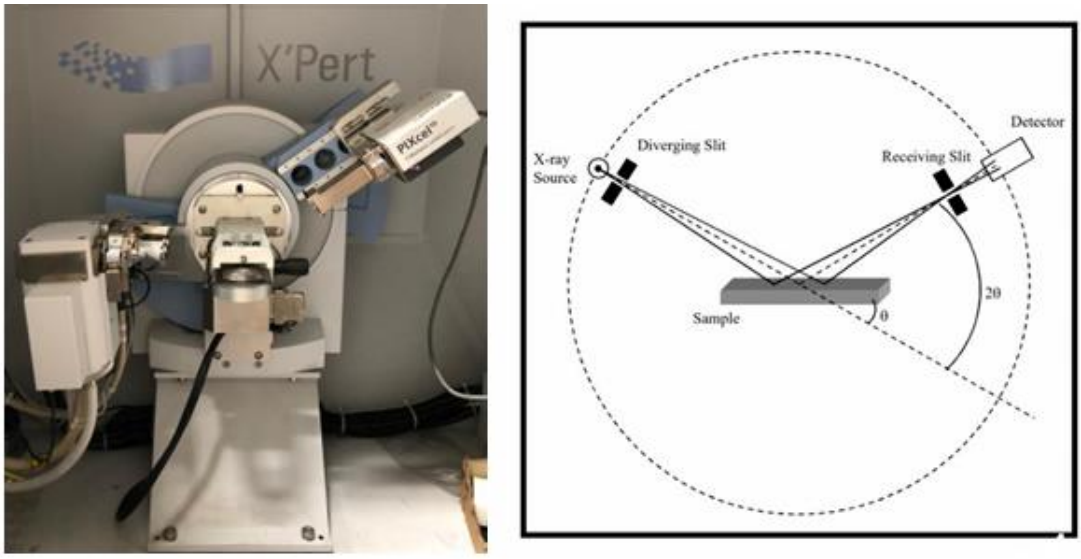

(a) Real XRD experimental set-up (b) Schematization of XRD apparatus

Figure 2-5 Real (a) and corresponding schematic (b) illustration of XRD device.

Finally, by comparison of an unknown sample's XRD data with standard reference XRD data for a known crystalline substance, unknown crystalline phases in a sample can be identified. Comparison of the reference data with the experimental XRD to identify whether all characteristic peaks are present is done in this way, for example, in Figure 2.6. Additionally, analysis of peak intensity can identify preferential sample orientation. If intensity of a specific diffraction peak is significantly higher than in the reference data, then the material preferentially has a certain crystallographic orientation on this plane.

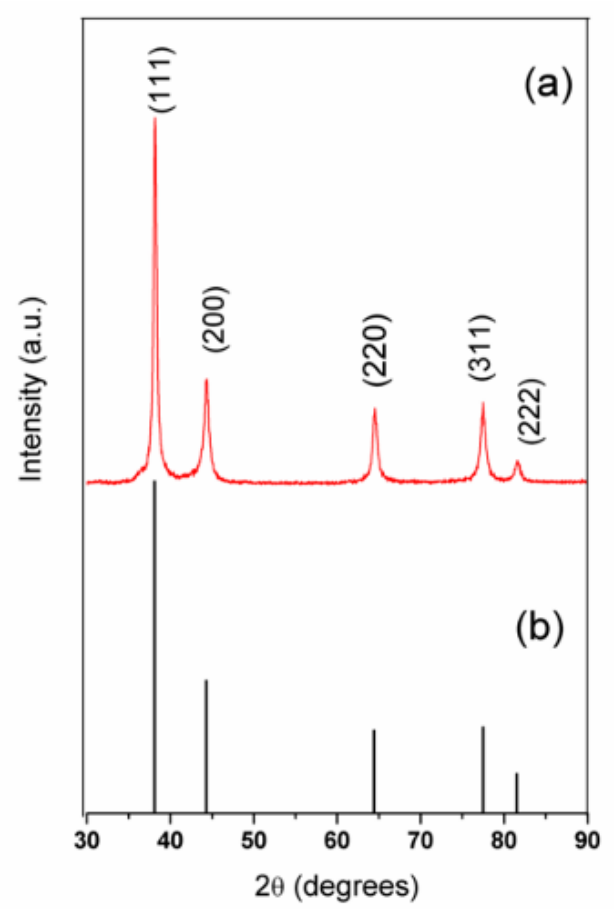

Figure 2-6-Example of XRD real spectrum (a) for Ag NPs and comparison with reference JCPDS file No. 04-0783

2.4. Electrode Fabrication:

Electrodes were prepared by the drop-casting technique, which is the most prevalent technique because it is simple to perform. In this technique, a liquid suspension of the material of interest particles is placed onto the substrate surface stepwise in single drops.

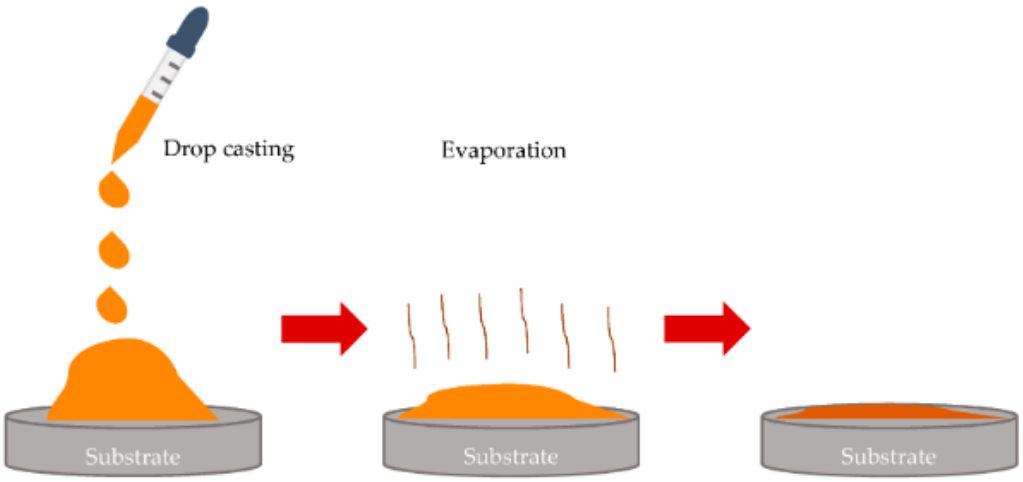

Figure 2-7 Drop casting method[40]

For this application GDL composed of carbon paper with Microporous Layer (MPL) which was treated with 5 wt% PTFE was used as basal composition material. One of sample results is shown in Figure 2.2. Drop casted suspension is Bi and Cu nano particles mixture in different loadings, Nafion and Iso propanol mixture. It is also worth noting that loadings of nano particles on GDL are 1.67 mg/cm^2. After solution evaporation electrode was placed on cathode base using copper tape for ensuring electric contact with base, and a teflon tape for marking electrode area of interest figure(2-8).

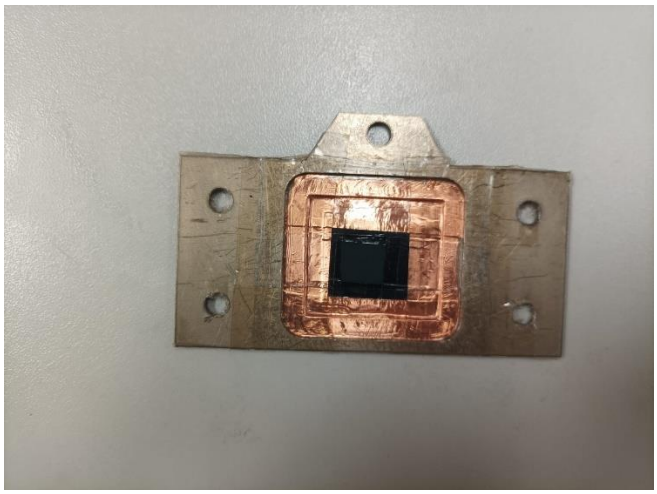

Figure 2-8 Catalyst on the cathode plate

2.5. Electrode Charachterization:

The electrodes were characterized using the following techniques:

1. Chronopotentiometry (CP) was utilized to quantify the CO_2 reduction reaction at controlled current densities.
2. High-Performance Liquid Chromatography (HPLC) and Gas Chromatography (GC) were utilized for identification and quantitation of the electrochemical products.
3. Cyclic voltammetry and Electrochemical Impedance Spectroscopy were employed to study the electrochemical properties and behavior of the electrodes.
4. X-ray Diffraction (XRD) was performed to determine the structural composition of the electrode materials

2.5.1. Chronopotentiometry

Chronopotentiometry or CP is an electrochemical technique to investigate how electrocatalysts work and are stable under constant current conditions (figure 2-9). Under CP measurements, a working electrode is applied with a constant current density and monitored for the resultant potential response of E vs. time. CP is a highly effective tool for electrocatalytic system assessment for electrocatalysts operating at real reaction rates, for example in CO_2 electroreduction. At the

beginning of the test, redox-active species begin to diffuse toward the working electrode in order to balance the electron flux flow. This continues until these species at the electrode surface reach zero concentration to reach the diffusion-limited state.

$$\boldsymbol{O + ne^{-} \rightleftarrows R} \quad \text{Eq 1-3}$$

Depending on the overall shape in Equation 2-4, when the surface concentration of electroactive species O is reduced to zero, the electrode potential will move towards more negative values. This occurs after some time interval, referred to as the transient time (τ). The transient time is proportional to both the diffusion coefficient of species O and to the initial solution concentration of this species.

$$\boldsymbol{\tau^{3/2} = \frac{2C_0^{*} nFAD_0^{1/2}}{3\beta}} \quad \text{Eq 2-4}$$

Where $C_0^{*} = \text{concentration}$ of O, n = electrons number, F=Faraday's Constant, A =working electrode area, D = diffusion coefficient, and β = sweep rate.

Chronopotentiometric measurements were carried out at room temperature using a CH 700E Series bipotentiostat. The measurements were conducted in a two-compartment electrochemical three-electrode cell using 1 M KOH as the electrolyte, represented schematically in Figure 2-10. Sustainion ion exchange membrane was used for cathodic and anodic compartment segregation. A sputter-coated IrO_2 counter electrode was employed and a leak-free Ag/AgCl (1 mm) electrode was used as the reference electrode.

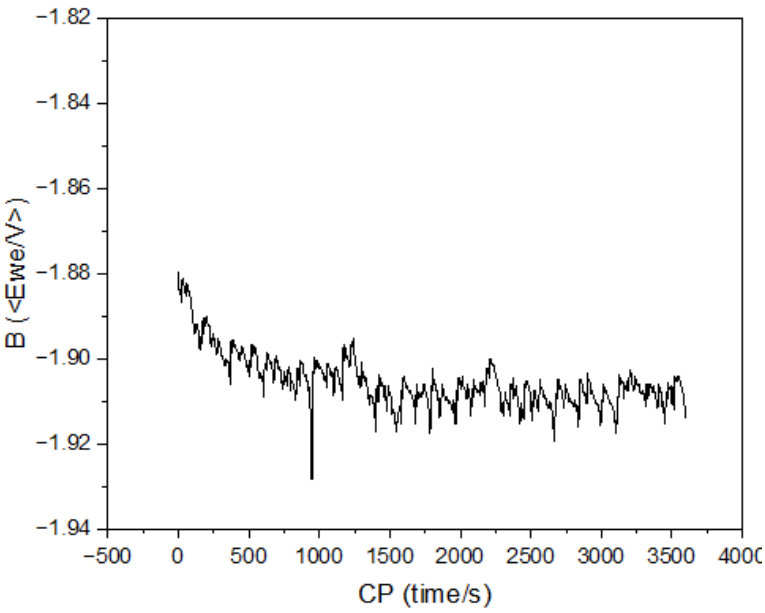

Figure 2-9 Typical obtained output from galvanostatic test.

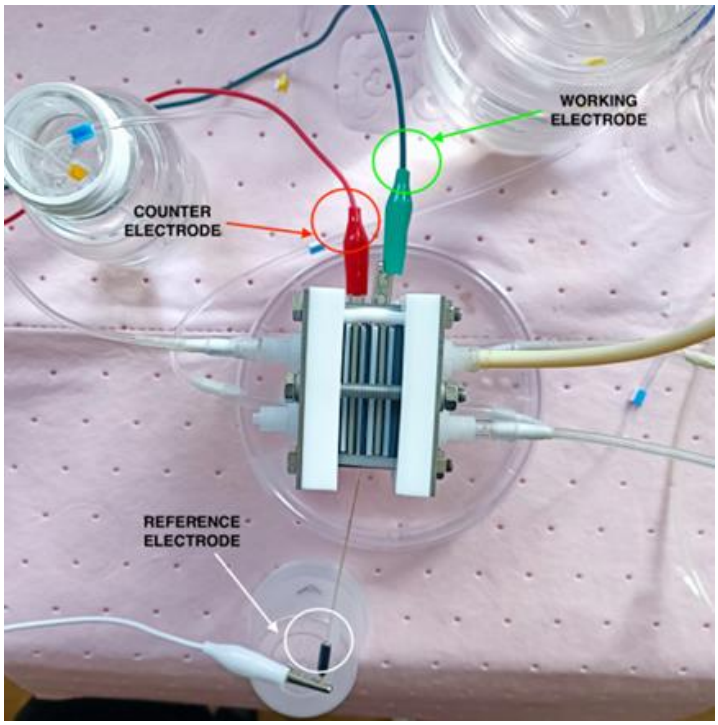

Figure 2-10-Three-electrode cell

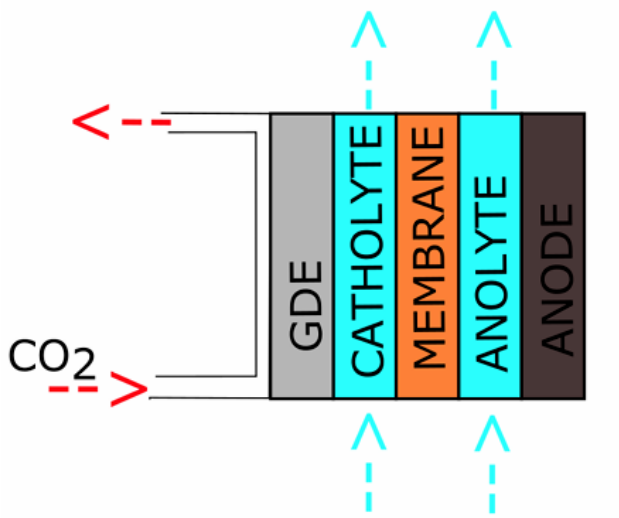

Figure 2-11 Membrane-based flow reactor

Figure 2-11 is a schematic representation of the electrochemical reactor. Carbon dioxide is fed at the back of the cathode, which is in the form of a gas diffusion electrode or GDE, to facilitate contact of the gaseous reactant with the catalytic surface. Electrolyte is passed through the cathodic and anodic chambers to facilitate ionic conductivity and electrochemical charge balancing.

2.5.2. High Performance Liquid Chromatography:

High-Performance Liquid Chromatography (HPLC) is a method of separation, identification, and quantitation of the constituents in a liquid sample. In electrochemical CO_2 reduction, HPLC is used to detect and measure liquid-phase products such as formic acid precisely and with high sensitivity.

The circuit diagram is given in figure 2-12:

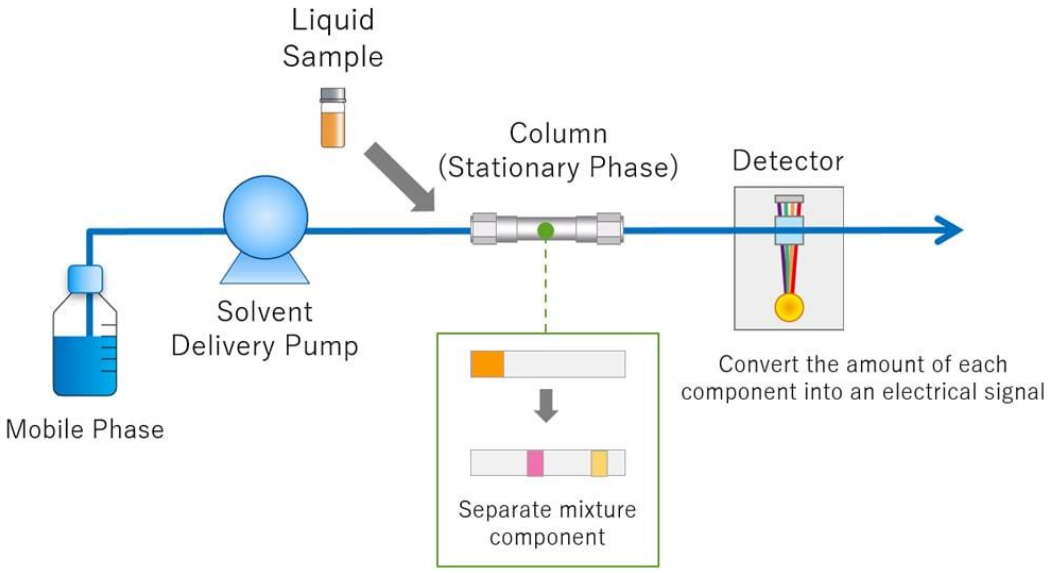

Figure 2-12 HPLC schematic

In HPLC, the mobile phase is driven through the system by a precision pump, which controls the flow rate to be in agreement with the needs of the detector. The liquid sample is injected and combined with the mobile phase by an injector, before being introduced into the column filled with the stationary phase. The analytes (compounds) in the mixture become separated as they move through the column, based on their various affinities to the stationary phase. After washout from the column, the analytes are detected and quantified by the detector (see Figure 2-13).

The outcome of analysis is graphed in chromatogram (Figure 2-14), every peak in which corresponds to a single compound. The retention time (t_a) is the time between sample injection and the appearance of a peak maximum, represented by the time when an analyte of interest reaches the detector. The dead time (t_0) is the time during which a non-retained species (a species that does not interact with the stationary phase) traverses the injector to the detector. For HPLC analysis, Thermo Fischer Ultimate 3000 was used. With UV-Vis detector at 210 nm on a Reprogel H^+ column (300 x 8 mm) with 9 mM H_2SO_4 (flow rate 1.0 mL min^{-1}) as the mobile phase. The FE with respect to liquid products in catholyte samples, taken at the beginning of every CP test, was calculated using Equation ---.

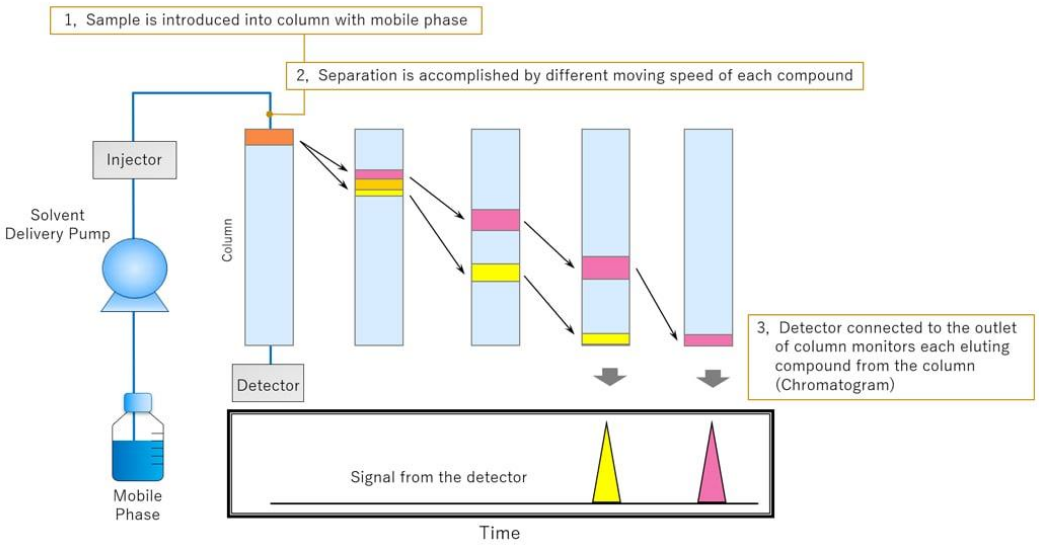

Figure 2-13 HPLC separation

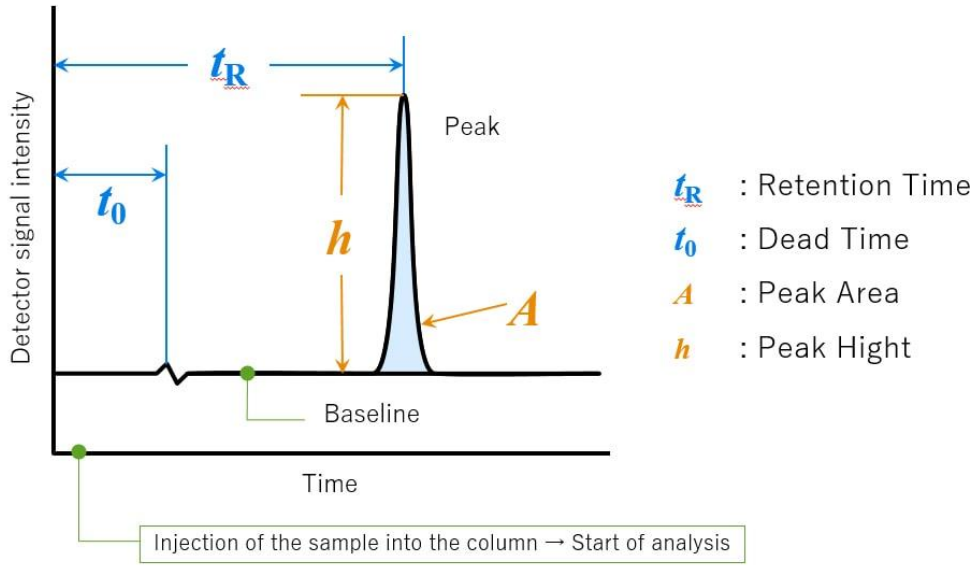

Figure 2-14 Chromatogram

$$\boldsymbol{FE = \frac{v*C*n*F}{Q}} \quad \text{Eq 2-5}$$

Where:

ν is the volume of catholyte (L);

C is the concentration of the liquid product ($molL^{-1}$);

n is the number of electrons required to obtain 1 molecule of this product;

F is the Faraday constant (96485 $Cmol^{-1}$);

Q is the total charge passed through the system during the CP test (coulombs, C).

2.5.3. Electrochemical Impedance Spectroscopy (EIS)

Electrochemical Impedance Spectroscopy (EIS) is a widely used technique for the examination of the interfacial properties and charge transfer mechanism of electrochemical systems. In EIS, a low AC voltage with a broad frequency range is applied in a sinusoidal wave form, and the impedance response of the system is measured. The technique provides valuable parameters such as solution resistance (Rs), charge transfer resistance (Rct), and double-layer capacitance (Cdl), which reflect the electrochemical activity of the interface between the electrode and electrolyte.

The impedance of a simplified Randles circuit is given by:

$$\boldsymbol{Z(\omega) = R_s + \frac{1}{\frac{1}{R_{ct}} + j\omega C_{dl}}} \quad \text{Eq 2-6}$$

Where:

R_s : the solution (electrolyte) resistance,

R_{ct} : the charge transfer resistance,

C_{dl} : the double-layer capacitance,

ω : the angular frequency,

j : the imaginary unit.

The data are typically graphed as a Nyquist plot with the x-axis representing real impedance (Z') and the y-axis imaginary (Z''). A semicircle in the Nyquist plot represents the charge transfer process, while the presence of a linear tail at the low frequencies suggests the presence of diffusion-related limitations.

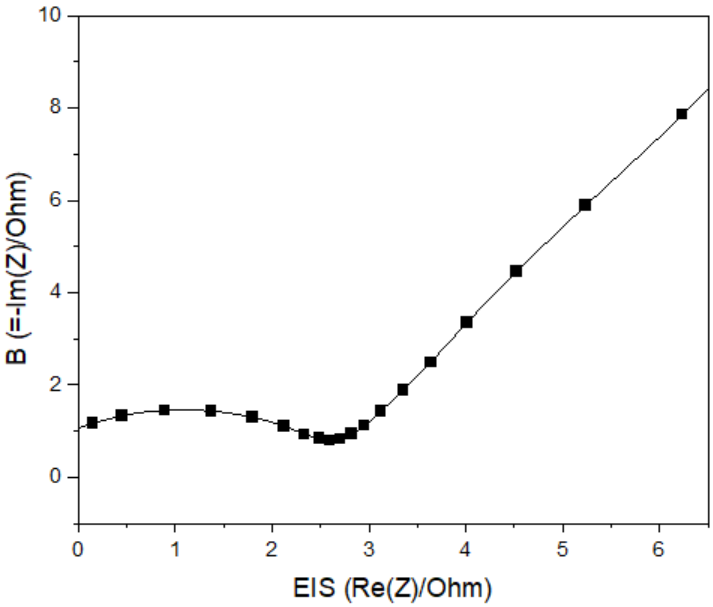

Figure 2-15 Typical obtained output from EIS test.

2.5.4. Linear Sweep Voltammetry (LSV)

Linear Sweep Voltammetry (LSV) is a widely used electrochemical technique for the examination of redox behavior of materials and the evaluation of the catalytic activity of electrodes. In LSV, the working electrode potential is scanned at a constant rate, and the resulting current is recorded against potential. LSV provides onset potential, over potential, and current density, essential parameters of electrocatalyst efficiency.

For diffusion-controlled redox reactions, the peak current (I_p) is described by the Randles–Ševčík equation at 25°C:

$$I_p = \left(2.69 \times 10^5\right).\ n^{3/2}.A.D^{1/2}.C.\ v^{1/2} \quad \text{Eq 2-7}$$

Where:

I_p: peak current (A)

n: number of electrons transferred,

A: electrode surface area (cm^2),

D: diffusion coefficient (cm^2/s),

C: concentration of the redox species (mol/cm^3),

v: scan rate (V/s).

By analyzing the LSV curves, key kinetic and mechanistic aspects of electrochemical reactions (such as CO_2 reduction or hydrogen evolution) can be determined.

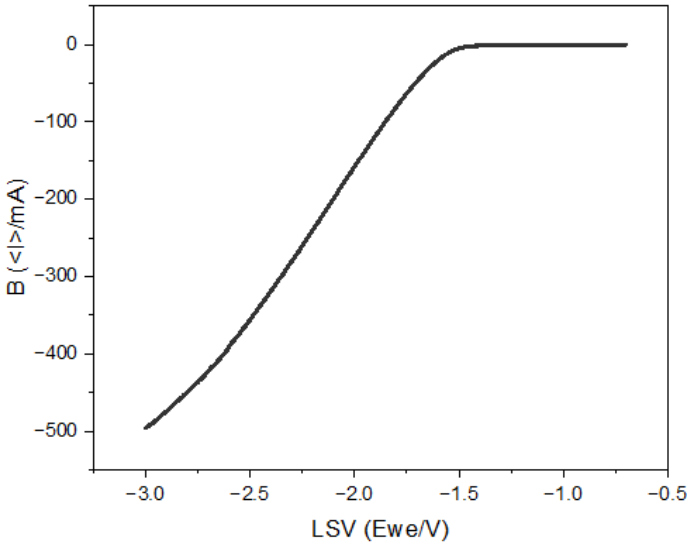

Figure 2-16 Typical obtained output from LSV test.

CHAPTER 3

3. Results and Discussion

The following are all the findings obtained from utilizing the methods outlined in the Chapter 2. The overall objective in this study was to explore the impact of bismuth on the electrochemical reduction of carbon dioxide (CO_2). Copper was employed as a standard catalyst due to its established activity for CO_2RR. To this end, both pure bismuth under different precursors and bismuth–copper composite catalysts (Bimetallic catalyst) were synthesized and evaluated in controlled atmospheres. Furthermore, with a view to achieving a better insight into the function of synthesis time on catalytic activity, pure bismuth samples were synthesized under diverse reaction times. This allowed comparative evaluation of their structural and electrochemical properties, which provided additional insight into the influence of bismuth in improving CO_2 conversion efficiency. For each selected catalyst, the electrochemical characterization is presented along with the morphological and compositional analysis achieved through FESEM. Additionally, the corresponding XRD results are discussed at the end of each section.

3.1. Bi-Based Catalyst

A number of recent reports have elucidated the excellent performance of Bi_2O_3 and Bi_2S_3 nanostructures in gas diffusion electrode (GDE) configuration. In particular, Monti and et al synthesized Bi_2O_3 nanostructures via a microwave-assisted green synthesis route that produced high surface area material capable of attaining Faradaic efficiencies (FE) of higher than 95% for HCOOH production over the broad pH range of pH 2–14. Notably, with 400 $mAcm^{-2}$ current density and pH 2, HCOOH selectivity was improved from 68% to 95%, while CO selectivity remained below 3%. Additionally, at highly basic pH (14), Bi_2O_3 formed as dendritic hierarchical structure with double-layer capacitance increase by 100%, indicating improvement in electrochemically active surface area and therefore catalysis

3.2. Bi-different precursors

In this case, bismuth-based catalysts were synthesized from two chemical precursors, bismuth nitrate $Bi(NO_3)_3$ and bismuth chloride $BiCl_3$, to explore the function of precursor materials to

control structural, morphological, and catalytic properties of final materials. With these two synthesis pathways, we systematically investigated the impact of the nature of the bismuth salt on the synthesis and catalytic performance of the catalyst in the electrochemical reduction of CO_2. The outcome of these comparative syntheses, along with the corresponding electrochemical performance values, are referred to and interpreted in the following sections:

3.2.1. Materials Characteristic:

FESEM images of bismuth nitrate and bismuth chloride are presented below. In Fig 3-1(a), for the $BiCl_3$-derived sample, the particles are rod-like with an approximate average length of 3 µm and an approximate radius of 40 nm. On the other hand, in Fig 3-1(b) the $Bi(NO_3)_3$ catalyst attained is of layered morphology, apparently indicative of a definite morphological difference between the two material syntheses.

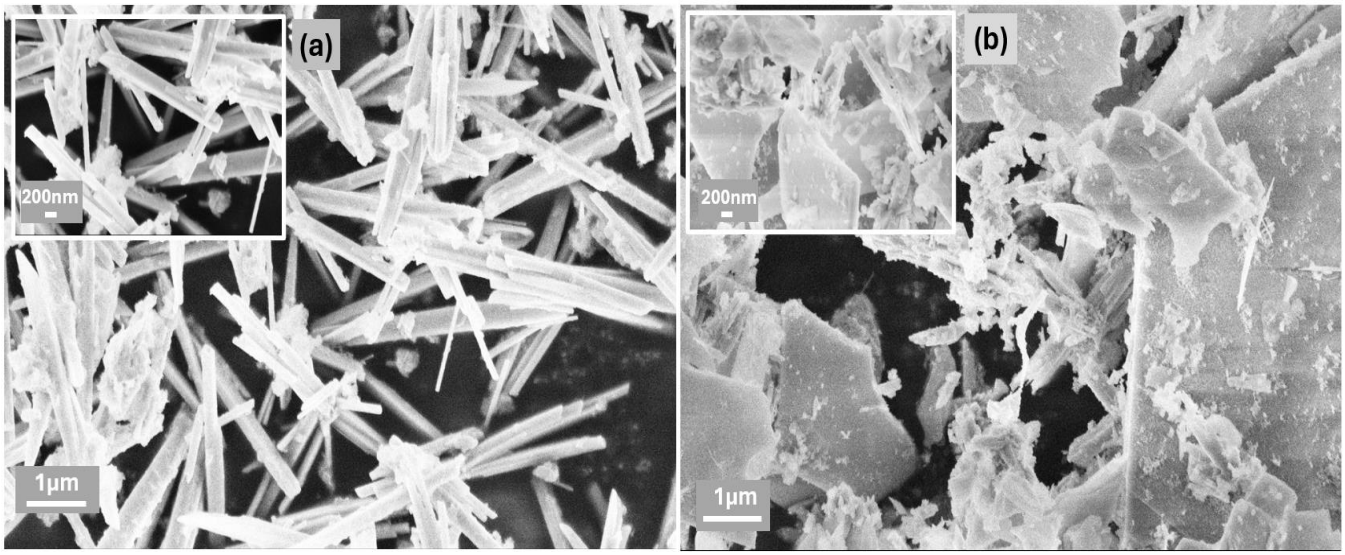

Figure 3-1- FESEM images of (a) $BiCl_3$ and (b) $Bi(NO_3)_3$

XRD spectra, shown in Fig3-2, were recorded to elucidate the crystalline character of synthesized compounds. From XRD patterns, By comparing the reference pattern it is found that the intense

diffraction maxima at 2θ = 22°, 25°, 28°, and 32° are well visible in both samples, thereby confirming the formation of the crystalline Bi_2S_3 phase successfully.

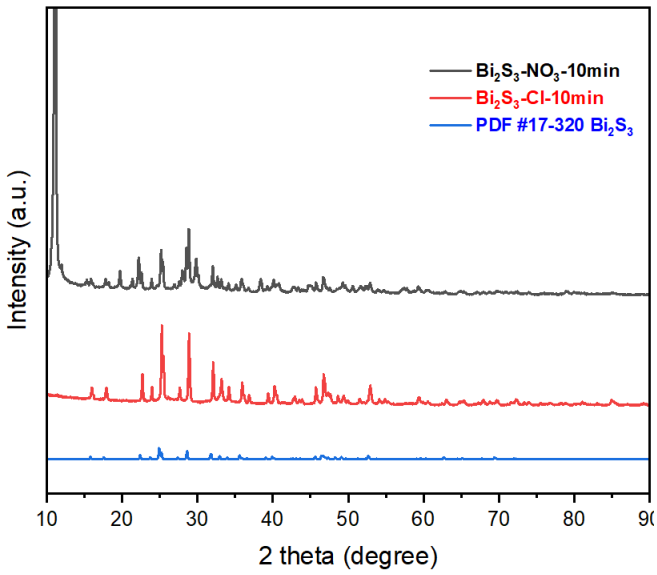

Figure 3-2- XRD of $BiCl_3$ and $Bi(NO_3)_3$

3.2.2. chrono-potentiometry

Figure 3-3 and 3-4 show the chrono-potentiometry curves of two catalysts at two current densities, 100 and 200 $mAcm^{-2}$, for an hour. Both catalysts exhibit stable operation; however, the $BiCl_3$-based catalyst is a little more negative in both current densities. These findings show that at both current densities whereas the $Bi(NO_3)_3$ precursor yields a little more energy efficiency, the $BiCl_3$ catalyst is more productive at 100 $mAcm^{-2}$,Whereas the $Bi(NO_3)_3$ showed more liquid productivity in 200 $mAcm^{-2}$, as will be discussed in the subsequent sections.

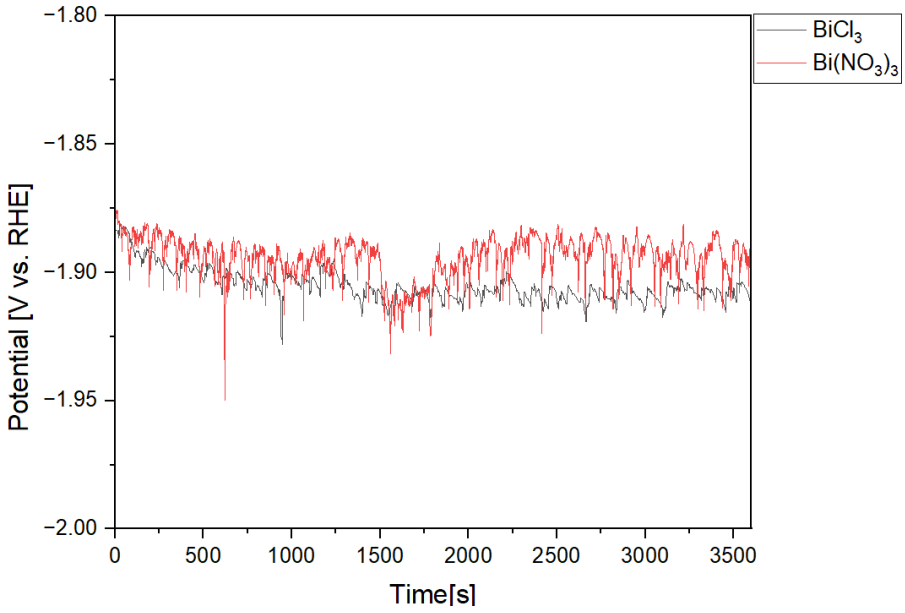

Figure 3-3- Chrono-potentiometry of the two catalysts at the current density of 100mAcm^{-2}

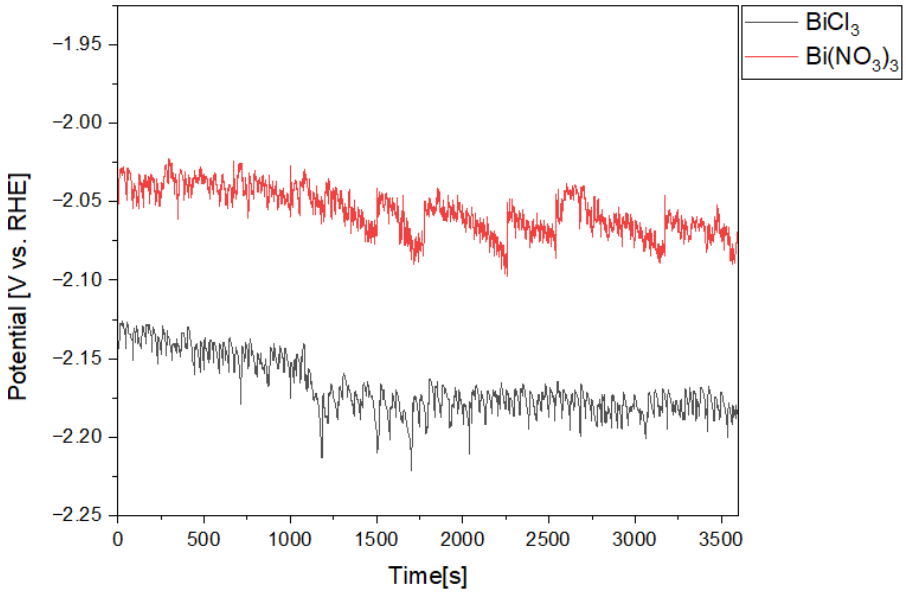

Figure 3-4- Chrono-potentiometry of the two catalysts at the current density of 200mAcm^{-2}

3.2.3. Faradaic Efficiency

As evident from the Faradaic efficiency graph (Figure 3-5), at 100 $mAcm^{-2}$ current density, the Bismuth catalyst developed (at ten minutes reaction time) using $BiCl_3$ precursor was more efficient compared to that developed using $Bi(NO_3)_3$ with around 90% formic acid generation. Which is in accordance with the amount of liquid product reported Monti and et al [41]. On the other hand, Fig 3-6, the catalyst prepared using $Bi(NO_3)_3$ displayed enhanced formic acid selectivity of 95%. The findings show that the choice of precursor can have a significant influence on product distribution and selectivity of the CO_2 reduction reaction at different current densities.

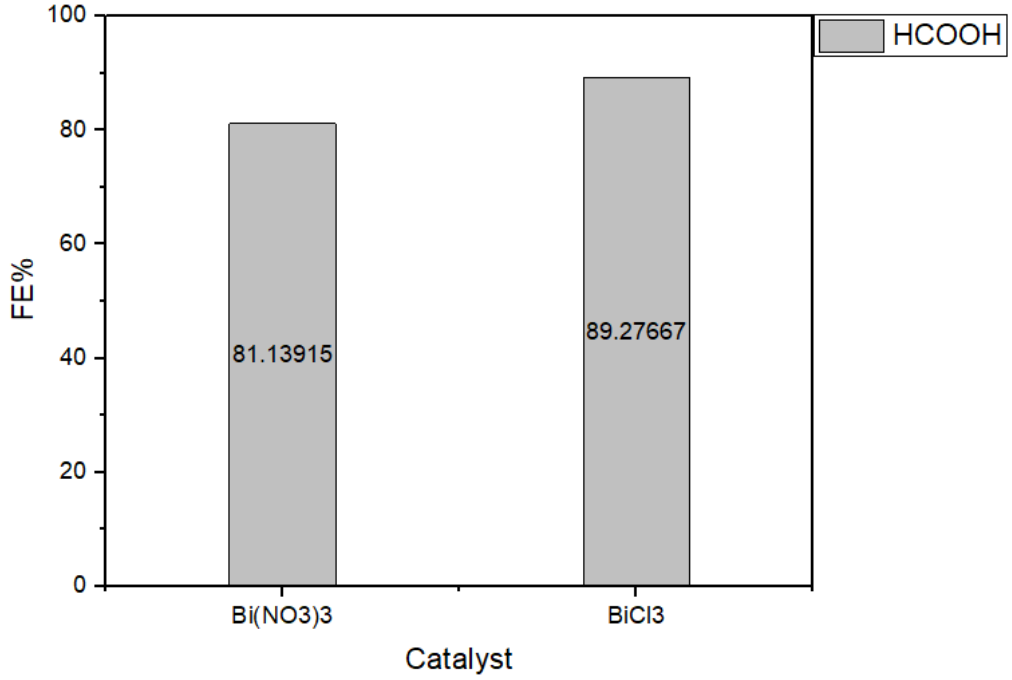

Figure 3-5- Faradaic efficiency at 100$mAcm^{-2}$

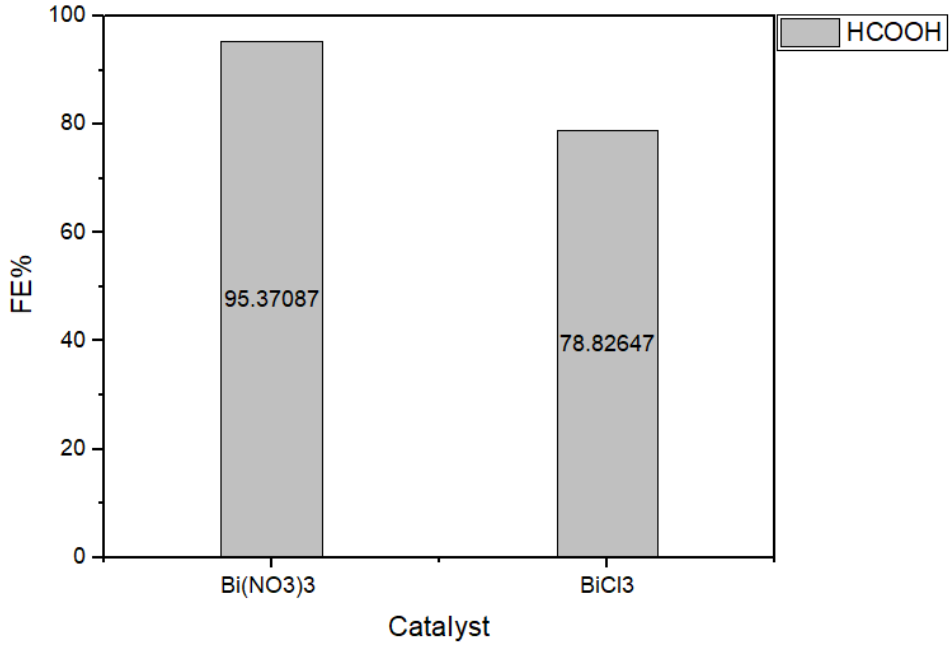

Figure 3-6- Faradaic efficiency at 200mAcm^{-2}

Table 3-1- Comparison of Faradaic Efficiency Between $BiCl_3$ and $Bi(NO_3)_3$ Derived Catalysts

Catalyst / Current density	$BiCl_3$	$Bi(NO_3)_3$
100 mAcm^{-2}	90%	80%
200 mAcm^{-2}	79%	95%

Subsequent investigations in this study focused primarily on the bismuth catalyst synthesized using the $BiCl_3$ precursor.

3.3. $BiCl_3$ Synthesis time

In this work, the performance of bismuth catalysts synthesized using $BiCl_3$ precursor is studied as a function of reaction time. Specifically, catalysts made for a reaction time of 2, 5, and 10 minutes are considered, and the findings presented and discussed below.

3.3.1. Materials Characteristic:

Figure 3-7 below show the FESEM images of bismuth catalysts prepared using $BiCl_3$ and reaction times of 2 minutes, 5 and 10 minutes, respectively. Clearly, all three samples have a nanowire morphology.

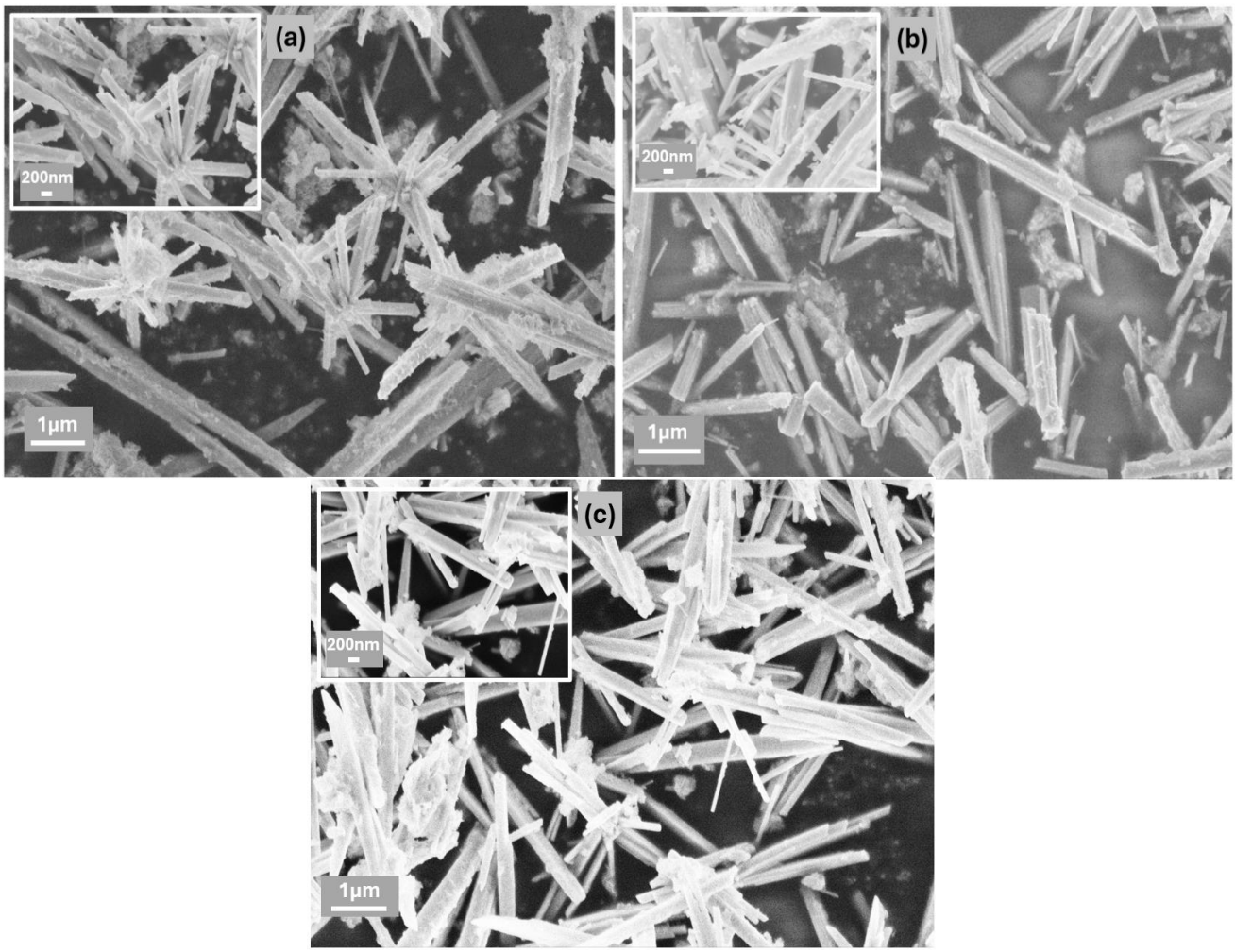

Figure 3-7- FESEM images of $BiCl_3$ at 2 minutes (a) 5 minutes (b) and 10 minutes (c)

As seen from the XRD pattern, Fig 3-8, comparison with the standard pattern of Bi_2S_3 reveals clear diffraction peaks at 22°, 24°, 28°, and 46°, which proves the successful crystallization and correct formation of the prepared samples.

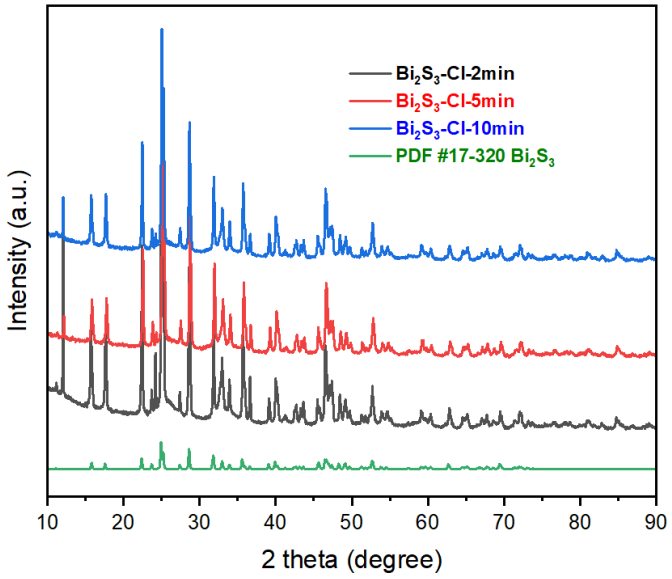

Figure 3-8- XRD of $BiCl_3$ at 2, 5 and 10 minutes

3.3.2. Chrono-Potentiometry

To study the effect of reaction time on the activity of $BiCl_3$-derived bismuth catalysts, chronopotentiometry (CP) tests were conducted at two current densities of 100 $mAcm^{-2}$ and 200 $mAcm^{-2}$ for catalysts synthesized with reaction times of 2, 5, and 10 minutes.

As observed from Figure 3-9 (100 $mAcm^{-2}$), all three catalysts display relatively stable potential profiles over the one-hour test period with minor fluctuations. The catalyst synthesized in 10 minutes possesses an average potential of approximately –1.89 V vs. RHE, which is a little more negative than that synthesized at 5 minutes (–1.85 V) and 2 minutes (–1.88 V). These differences, although small, suggest that longer reaction times can lead to more electrochemically active surfaces at low current densities.

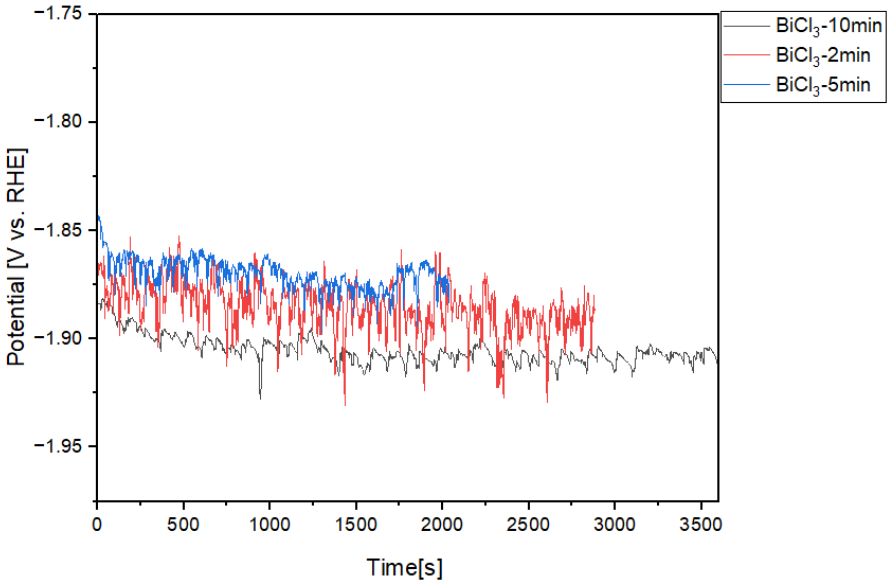

Figure 3-9- Chrono-potentiometry of the three catalysts at the current density of 100mAcm^{-2}

At higher current density of 200 mAcm^{-2}, as indicated in Figure 3-10, differences in potential behavior and stability become more pronounced. The catalyst synthesized at 5 minutes exhibits a much lower and more negative potential with an average value of –2.28 V and with detectable drift with time. This could be indicative of either higher activity or potential instability under high-load conditions. In contrast, the 2 minute and 10 minute catalysts operate at more stable potentials of around –2.15 V and –2.13 V, respectively, with less indication of degradation or fluctuation.

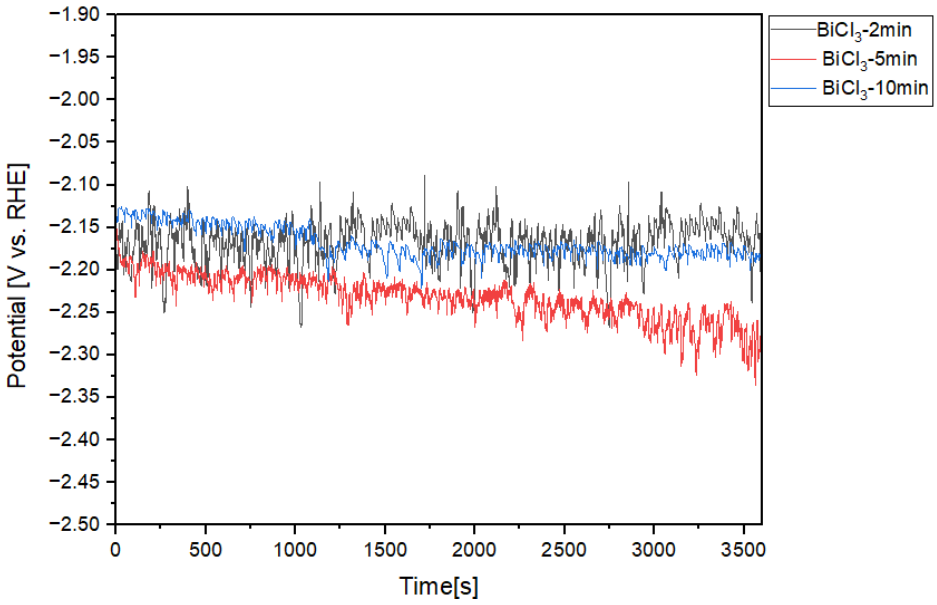

Figure 3-10- Chrono-potentiometry of the three catalysts at the current density of 200mAcm^{-2}

3.3.3. Faradaic Efficiency

As is seen from Figure 3-11, at 100 mAcm^{-2} of the current density, formic acid (HCOOH) Faradaic efficiency is increasing with longer reaction times constantly, from 70.33% for the 2-minute catalyst to 89% for the 10-minute catalyst. Surprisingly, only the 10-minute catalyst was prepared in this way. The better product selectivity highlight the better catalytic performance of the 10-minute $BiCl_3$-derived catalyst under these reaction conditions.

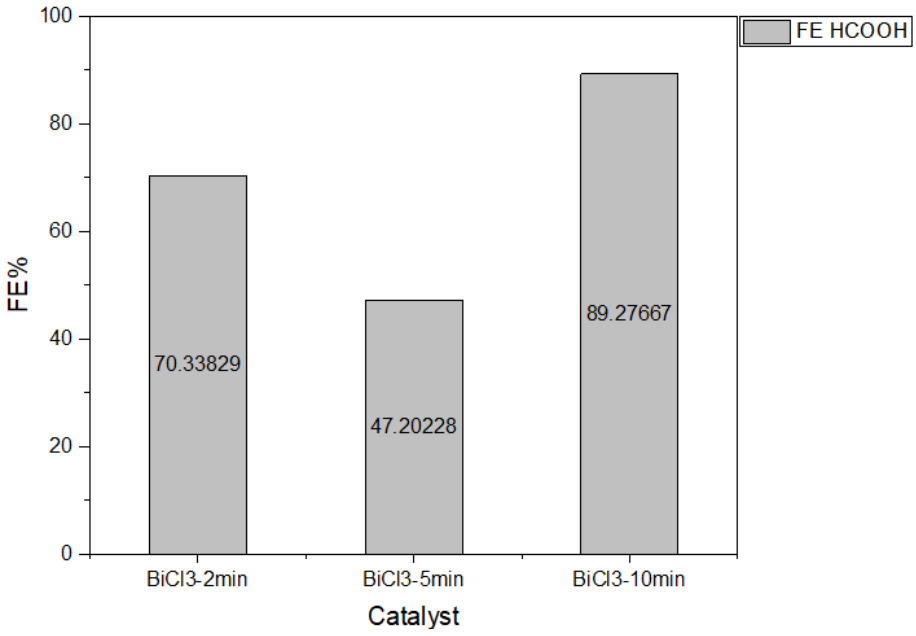

Figure 3-11- Faradaic efficiency of catalysts in 3 different reaction time at 100mAcm^{-2}

As observed from Figure 3-12, at 200 mAcm^{-2} current density, the catalyst made using a 10-min reaction time again outperforms the 2-min sample by recording a higher Faradaic efficiency of 78.82% rather than 65.41%. This again verifies the positive effect of longer reaction time on catalytic efficiency under greater stress on current.

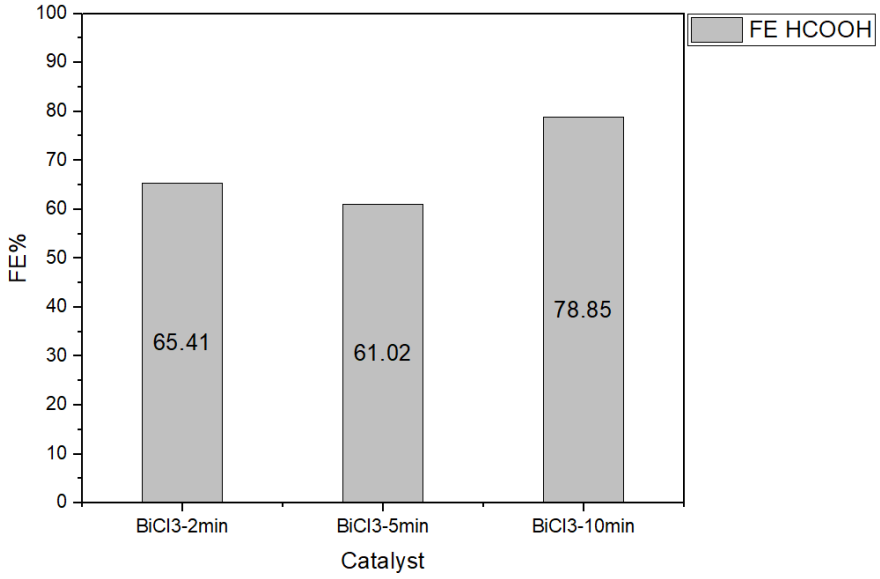

Figure 3-12- Faradaic efficiency of catalysts in 3 different reaction time at 200mAcm^{-2}

3.4. Bi-Cu bimetallic catalyst

According to the results in the previous section, bimetallic Bi–Cu catalysts were prepared using $BiCl_3$ and $CuCl_2$ as corresponding precursors. For this part of the study, various molar ratios of the two precursors were prepared and electrochemically tested in order to measure their catalytic activity. The respective results and discussions are presented in the following sections.

3.4.1. Materials characteristic

As shown below, the FESEM images and XRD analysis for the bimetallic catalysts synthesized using $BiCl_3$ and $CuCl_3$ with different concentration ratios (9:1, 0.5:0.5, 1:9 and 0.05:0.95) as well as pure $CuCl_2$, are presented in Figures 3-13 and 3-14 respectively.

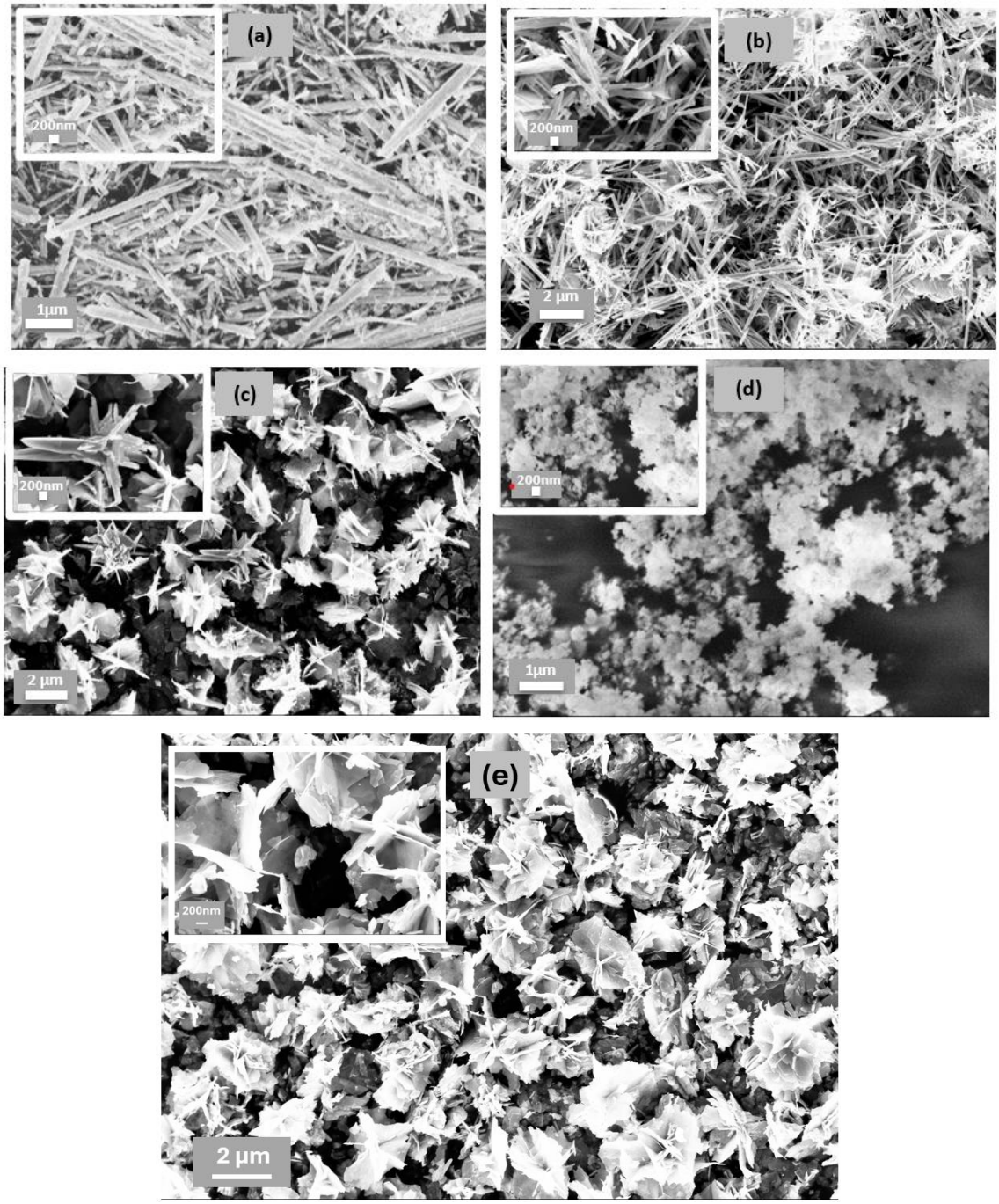

Figure 3-13- FESEM images of Bimetallic at different ratios at Bi 9:1 Cu(a) Bi 0.5:0.5 Cu (b) Bi 1:9 Cu (c) $CuCl_2$ (d) and Bi0.05:0.95 Cu (e)

As evident from the XRD patterns presented, the sample synthesized using copper chloride exhibits clear peaks at 2θ = 31°, 48°, and 59° that are well matched with the reference pattern of CuS (PDF #1-1281), indicating successful development of this phase. Further, in the bimetallic samples, and particularly the ones with a greater copper ratio like $Cu_{0.95}Bi_{0.05}$, these CuS characteristic peaks remain readily discernible, suggesting that the copper phase remains predominant in such compositions.

Conversely, peaks around 2θ = 24°, 28°, and 46°, which match the reference pattern of Bi_2S_3 (PDF #17-320), are distinctly observed in higher bismuth content samples, such as Bi_9Cu_1. Such peaks are evidence of the presence of crystalline Bi_2S_3 in these compositions. Overall, the occurrence of CuS and Bi_2S_3 phases in varying intensities in the different samples is indicative of the successful creation of bimetallic structures, and also suggests that the composition of the crystalline phases is directly proportional to the ratio of the precursors used.

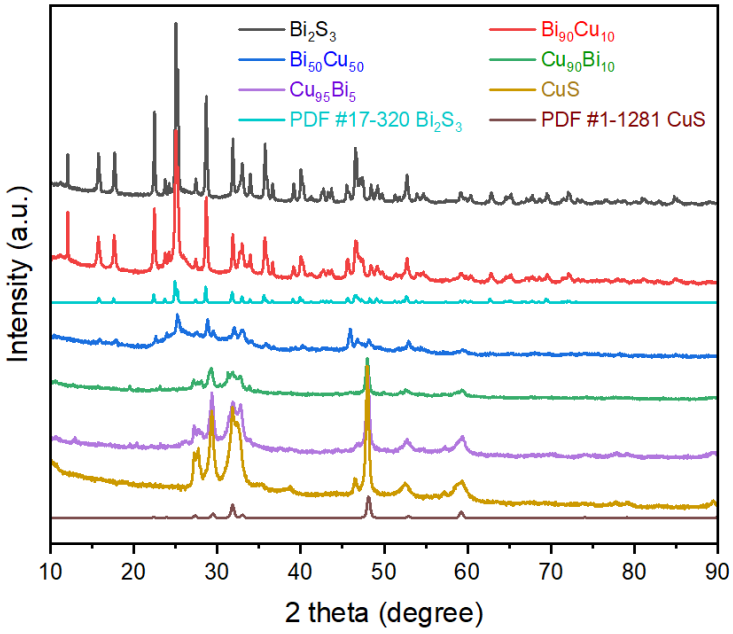

Figure 3-14- XRD analysis of $BiCl_3$ and $CuCl_3$ with different concentration ratios

3.4.2. Chrono-potentiometry

Figures 3-15 and 3-16 present the chrono-potentiometry (CP) curves for the bimetallic Bi–Cu catalysts at current densities of 100 and 200 $mAcm^{-2}$, respectively. As observed, all samples exhibit relatively stable and consistent potential profiles over the duration of the tests, indicating good electrochemical stability and reliable experimental conditions across both current densities.

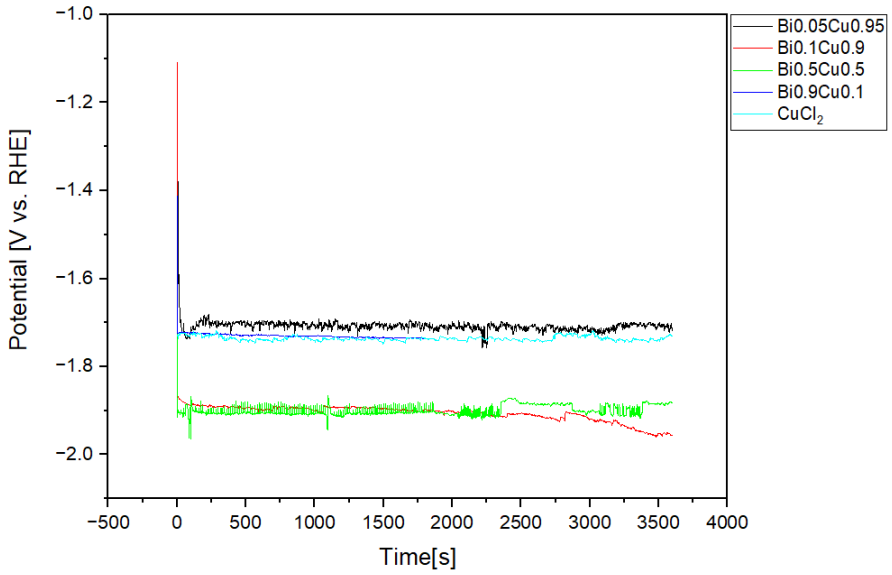

Figure 3-15- Chrono-potentiometry of the catalyst with different ratios of Bi and Cu at the current density of 100$mAcm^{-2}$

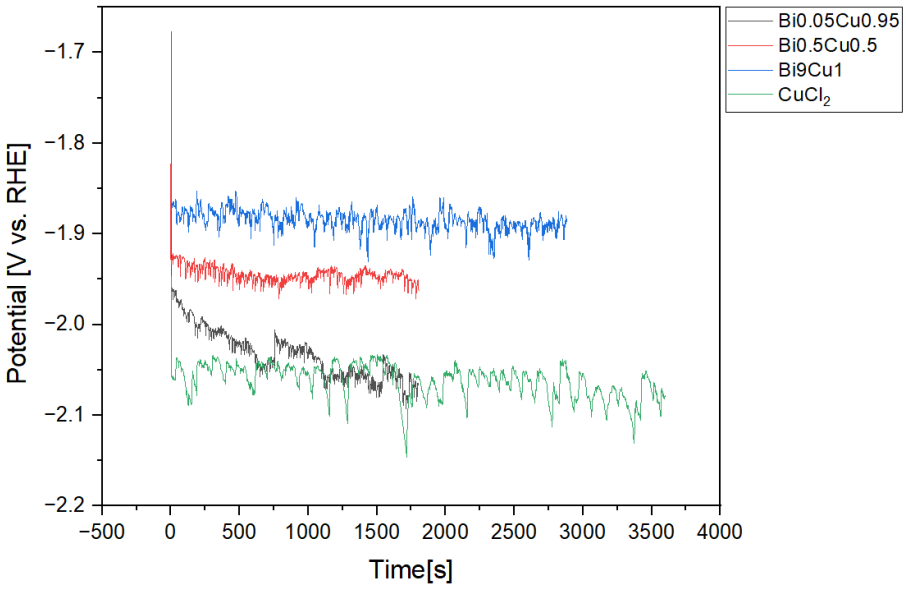

Figure 3-16- Chrono-potentiometry of the catalyst with different ratios of Bi and Cu at the current density of 200$mAcm^{-2}$

3.4.3. Faradaic Efficiency

Figures 3-17 and 3-18 illustrate the Faradaic efficiencies (FE) for formic acid and acetic acid production at current densities of 100 and 200 $mAcm^{-2}$, respectively, for various Bi–Cu bimetallic catalysts.

At the current density of 100 mA cm^{-2}, there is a clear disparity in Faradaic efficiency (FE) for formic acid production among different catalysts. The pure $BiCl_3$ catalyst is the best performing with an impressive FE of 89.27%, demonstrating the superior inherent activity of the catalyst towards selective electroreduction of CO_2 to formic acid. $CuCl_2$ is also very good with an FE of 80.56%, ranking second-best among the studied materials.

Among the bimetallic catalysts, $Bi_{0.9}Cu_{0.1}$ composition exhibits best performance, delivering an FE of 70.22%, which is greater than other Bi–Cu compositions. This suggests that addition of a small quantity of copper into the structure of bismuth enhances catalytic efficiency, likely via synergistic effects of activation of CO_2 and product selectivity.

For comparison, $Bi_{0.5}Cu_{0.5}$ and $Bi_{0.1}Cu_{0.9}$ exhibited 69.17% and 61.25% FE, respectively, while $Bi_{0.05}Cu_{0.95}$ was at 67.87%. Although no bimetallic system was superior to pure $BiCl_3$ in formic acid selectivity, $Bi_{0.9}Cu_{0.1}$ was the best among the bimetallic catalysts and evidently a large Bi-to-Cu ratio is conducive to the effective conversion of CO_2 under such circumstances.

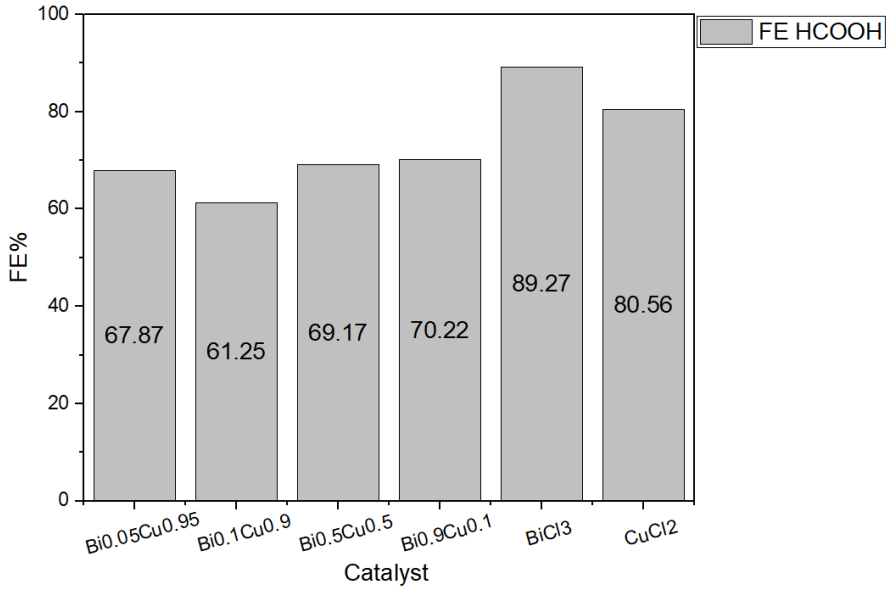

Figure 3-17- faradaic efficiency of the catalyst with different ratios of Bi and Cu at the current density of 100mAcm^{-2}

At 200 mA cm^{-2} , the overall trend for Faradaic efficiency (FE) for formic acid production is marginally deviating from that at the 100 mA cm^{-2} condition. The $Bi_{0.9}Cu_{0.1}$ catalyst is now at the forefront with a top FE of 80.9%, even beating pure $BiCl_3$ and $CuCl_2$ with 76.34% and 75.5%, respectively. This indicates that the bimetallic system with dominant Bi ratio not only retains but also enhances catalytic activity at higher current densities, due to apparently improved CO_2 activation kinetics as well as stabilization of significant intermediates.

In contrast, the other bimetallic alloys such as $Bi_{0.5}Cu_{0.5}$ and $Bi_{0.05}Cu_{0.95}$ exhibit a steep drop in FE to 39.03% and 43.6%, respectively. The loss of performance at high current density suggests that higher Cu content may not be beneficial for formic acid selectivity in these demanding conditions and is likely due to competitive HER or poorer surface stability.

Therefore, the $Bi_{0.9}Cu_{0.1}$ catalyst not only exhibits superior bimetallic activity at 100 mA cm^{-2} but also surpasses all the tested catalysts at 200 mA cm^{-2} proving that composition adjustment plays a significant role in improving bimetallic electrocatalysts for effective CO_2 electroreduction.

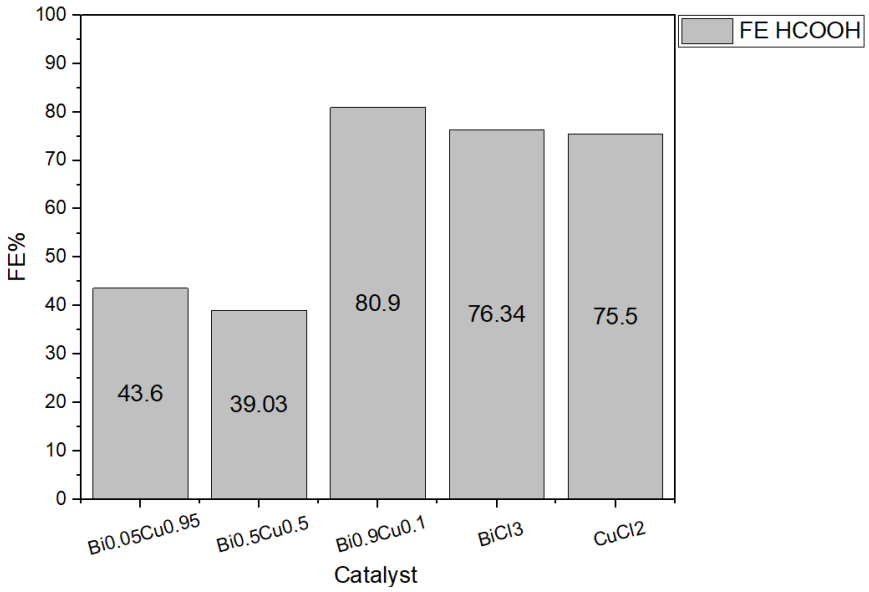

Figure 3-18- faradaic efficiency of the catalyst with different ratios of Bi and Cu at the current density of 200mAcm^{-2}

CHAPTER 4

4. CONCLUSION

A series of bismuth and bismuth–copper bimetallic electrocatalysts were synthesized and investigated for CO_2 electrochemical reduction to value-added chemicals,like Formic acid. Three major variables were investigated in the study: type of bismuth precursor, synthesis reaction duration, and Bi–Cu ratio of bimetallic ratios.

First, precursor choice was found to have a significant impact on catalytic performance. The $BiCl_3$-derived catalyst was observed to be significantly more active than that based on $Bi(NO_3)_3$, and it achieved an almost 90% FE for formic acid at 100 $mAcm^{-2}$, consistent with past results. Although the $Bi(NO_3)_3$ sample proved to be marginally more selective (up to 95%) in some isolated cases, the $BiCl_3$-derived material yielded more reproducible and stable results, particularly at high current densities.

Second, the reaction time for synthesis was a critical factor. The doubling of the reaction time from 2 to 10 minutes significantly improved the catalytic activity. The 10-minute $BiCl_3$-derived catalyst achieved a maximum FE of 89% at 100 $mAcm^{-2}$ and 78.82% at 200 $mAcm^{-2}$, both values greater than the 2-minute sample. This is attributed to enhanced crystallinity and growth of the nanostructure, as indicated from FESEM and XRD investigations.

Finally, the addition of copper to the bismuth framework caused considerable variations in the performance. Out of the bimetallic systems, the $Bi_{0.9}Cu_{0.1}$ showed the most promising results throughout, 70.22% and 80.9% FE for formic acid at current densities of 100 and 200 $mAcm^{-2}$, respectively. These findings show a high-order synergistic effect between copper and bismuth when the bismuth fraction remains dominating. Conversely, catalysts with higher copper ratios incurred significant losses in efficiency, likely due to competitive side reactions such as hydrogen evolution and structural instability at higher loads of current.

In summary, the study reveals that the control of precursor type, reaction time, and bimetallic composition can greatly influence activity and selectivity of electrocatalysts for the CO_2 reduction. The $BiCl_3$-based catalyst prepared with a synthesis time of 10 minutes, particularly when combined with sufficient copper, presents an extremely promising pathway towards selective and efficient electrochemical CO_2 conversion.

Reference

1. Zheng, Y., et al., *Understanding the roadmap for electrochemical reduction of CO2 to multi-carbon oxygenates and hydrocarbons on copper-based catalysts.* Journal of the American Chemical Society, 2019. **141**(19): p. 7646-7659.
2. Liang, S., et al., *Electrolytic cell design for electrochemical CO2 reduction.* Journal of CO2 Utilization, 2020. **35**: p. 90-105.
3. Whipple, D.T., E.C. Finke, and P.J. Kenis, *Microfluidic reactor for the electrochemical reduction of carbon dioxide: the effect of pH.* Electrochemical and Solid-State Letters, 2010. **13**(9): p. B109.
4. Yoro, K.O. and M.O. Daramola, *CO2 emission sources, greenhouse gases, and the global warming effect*, in *Advances in carbon capture*. 2020, Elsevier. p. 3-28.
5. Jiao, S., et al., *The lab-to-fab journey of copper-based electrocatalysts for multi-carbon production: Advances, challenges, and opportunities.* Nano Today, 2021. **36**: p. 101028.
6. Caetano, M.A.L., D.F.M. Gherardi, and T. Yoneyama, *Optimal resource management control for CO2 emission and reduction of the greenhouse effect.* Ecological Modelling, 2008. **213**(1): p. 119-126.
7. Tufa, R.A., et al., *Towards highly efficient electrochemical CO2 reduction: Cell designs, membranes and electrocatalysts.* Applied Energy, 2020. **277**: p. 115557.
8. Xing, Z., et al., *Enhancing carbon dioxide gas-diffusion electrolysis by creating a hydrophobic catalyst microenvironment.* Nature communications, 2021. **12**(1): p. 136.
9. Peterson, A.A., et al., *How copper catalyzes the electroreduction of carbon dioxide into hydrocarbon fuels.* Energy & Environmental Science, 2010. **3**(9): p. 1311-1315.
10. Hernández, S., et al., *Syngas production from electrochemical reduction of CO 2: current status and prospective implementation.* Green Chemistry, 2017. **19**(10): p. 2326-2346.
11. Liu, C.-C., *An extended method for key factors in reducing CO2 emissions.* Applied Mathematics and Computation, 2007. **189**(1): p. 440-451.
12. Pei, Y., H. Zhong, and F. Jin, *A brief review of electrocatalytic reduction of CO2—Materials, reaction conditions, and devices.* Energy Science & Engineering, 2021. **9**(7): p. 1012-1032.
13. Garg, S., et al., *Advances and challenges in electrochemical CO 2 reduction processes: an engineering and design perspective looking beyond new catalyst materials.* Journal of Materials Chemistry A, 2020. **8**(4): p. 1511-1544.

14. Zhong, H., et al., *Effect of CO2 bubbling into aqueous solutions used for electrochemical reduction of CO2 for energy conversion and storage.* The Journal of Physical Chemistry C, 2015. **119**(1): p. 55-61.
15. Kalyanasundaram, K., *Photochemical and photoelectrochemical approaches to energy conversion.* Dye-sensitized solar cells, 2010. **1**: p. 1-38.
16. Zhang, J., et al., *Tandem effect of Ag@ C@ Cu catalysts enhances ethanol selectivity for electrochemical CO2 reduction in flow reactors.* Cell Reports Physical Science, 2022. **3**(7).
17. Hao, D., et al., *Boosted selective catalytic nitrate reduction to ammonia on carbon/bismuth/bismuth oxide photocatalysts.* Journal of Cleaner Production, 2022. **331**: p. 129975.
18. Kauffman, D.R., et al., *Selective electrocatalytic reduction of CO2 into CO at small, thiol-capped Au/Cu nanoparticles.* The Journal of Physical Chemistry C, 2018. **122**(49): p. 27991-28000.
19. Gupta, N.D., *Periodic Nanophotonic Structures-Based Light Management for Solar Energy Harvesting*, in *Optoelectronics*. 2020, IntechOpen.
20. Wang, X., et al., *Enhanced Electroconversion CO2-to-Formate by Oxygen-Vacancy-Rich Ultrasmall Bi-Based Catalyst Over a Wide Potential Window.* ChemCatChem, 2022. **14**(6): p. e202101873.
21. Rasul, S., et al., *A highly selective copper–indium bimetallic electrocatalyst for the electrochemical reduction of aqueous CO2 to CO.* Angewandte Chemie International Edition, 2015. **54**(7): p. 2146-2150.
22. Larrazábal, G.O., et al., *Analysis of mass flows and membrane cross-over in CO2 reduction at high current densities in an MEA-type electrolyzer.* ACS applied materials & interfaces, 2019. **11**(44): p. 41281-41288.
23. Vermaas, D.A. and W.A. Smith, *Synergistic electrochemical CO2 reduction and water oxidation with a bipolar membrane.* ACS Energy Letters, 2016. **1**(6): p. 1143-1148.
24. Lee, S., et al., *Alkaline CO2 electrolysis toward selective and continuous HCOO–production over SnO2 nanocatalysts.* The Journal of Physical Chemistry C, 2015. **119**(9): p. 4884-4890.
25. Ooka, H., M.C. Figueiredo, and M.T. Koper, *Competition between hydrogen evolution and carbon dioxide reduction on copper electrodes in mildly acidic media.* Langmuir, 2017. **33**(37): p. 9307-9313.
26. Seh, Z.W., et al., *Combining theory and experiment in electrocatalysis: Insights into materials design.* Science, 2017. **355**(6321): p. eaad4998.

27. Jeanty, P., et al., *Upscaling and continuous operation of electrochemical CO2 to CO conversion in aqueous solutions on silver gas diffusion electrodes.* Journal of CO2 Utilization, 2018. **24**: p. 454-462.
28. Liu, X., et al., *Studying photocatalytic dye degradation with bismuth nitrate–derived catalysts using paper microzones method.* Materials Today Chemistry, 2022. **23**: p. 100667.
29. Marepally, B.C., et al., *Role of small Cu nanoparticles in the behaviour of nanocarbon-based electrodes for the electrocatalytic reduction of CO2.* Journal of CO2 Utilization, 2017. **21**: p. 534-542.
30. Al Harthi, A., et al., *Criteria and cutting-edge catalysts for CO_2 electrochemical reduction at the industrial scale.* Journal of CO2 Utilization, 2024. **83**: p. 102819.
31. Shadervan, A., et al., *Mechanistic understanding of asphaltene precipitation and oil recovery enhancement using SiO2 and CaCO3 nano-inhibitors.* Scientific Reports, 2024. **14**(1): p. 15249.
32. Jiang, Z., et al., *pH-Universal Electrocatalytic CO2 Reduction with Ampere-level Current Density on Doping-engineered Bismuth Sulfide.* Angewandte Chemie, 2024: p. e202408412.
33. Zeng, J., et al., *Novel insights into Sb-Cu catalysts for electrochemical reduction of CO2.* Applied Catalysis B: Environmental, 2022. **306**: p. 121089.
34. Bensmann, B., et al., *Optimal configuration and pressure levels of electrolyzer plants in context of power-to-gas applications.* Applied energy, 2016. **167**: p. 107-124.
35. Wang, M., et al., *Synergistic geometric and electronic effects in Bi–Cu bimetallic catalysts for CO2 electroreduction to formate over a wide potential window.* ACS Sustainable Chemistry & Engineering, 2022. **10**(17): p. 5693-5701.
36. Kortlever, R., et al., *Catalysts and reaction pathways for the electrochemical reduction of carbon dioxide.* The journal of physical chemistry letters, 2015. **6**(20): p. 4073-4082.
37. Deng, P., et al., *Metal–organic framework-derived carbon nanorods encapsulating bismuth oxides for rapid and selective CO2 electroreduction to formate.* Angewandte Chemie, 2020. **132**(27): p. 10899-10905.
38. Fan, K., et al., *Curved surface boosts electrochemical CO2 reduction to formate via bismuth nanotubes in a wide potential window.* Acs Catalysis, 2019. **10**(1): p. 358-364.
39. Liu, B., et al., *Copper-triggered delocalization of bismuth p-orbital favours high-throughput CO2 electroreduction.* Applied Catalysis B: Environmental, 2022. **301**: p. 120781.

40. Bormashenko, E., Y. Bormashenko, and M. Frenkel, *Formation of hierarchical porous films with breath-figures self-assembly performed on oil-lubricated substrates.* Materials, 2019. **12**(18): p. 3051.
41. Monti, N.B., et al., *Unveiling the Origin of pH-Dependent Catalytic Performance of Bi2O3 Nanostructure for Electrochemical CO2 Reduction.* The Journal of Physical Chemistry Letters, 2025. **16**(15): p. 3761-3768.